crystals

MDPI

Article

Novel Salts of Heterocyclic Polyamines and 5-Sulfosalicylic Acid: Synthesis, Crystal Structure, and Hierarchical Supramolecular Interactions

Joanna Bojarska [1], Krzysztof Łyczko [2] and Adam Mieczkowski [3,*]

[1] Institute of Faculty of Chemistry, Institute of General & Inorganic Chemistry, Technical University of Lodz, Zeromskiego 116, 90-924 Lodz, Poland; joanna.bojarska@p.lodz.pl
[2] Institute of Nuclear Chemistry and Technology, Dorodna 16, 03-195 Warsaw, Poland; k.lyczko@ichtj.waw.pl
[3] Institute of Biochemistry and Biophysics, Polish Academy of Sciences, Pawinskiego 5a, 02-106 Warsaw, Poland
* Correspondence: amiecz@ibb.waw.pl

Abstract: A series of novel salts of heterocyclic polyamines with 5-sulfosalicylic acid ($C_4H_7N_4^+$)($C_7H_5O_6S^-$)·2(H_2O) (**1**), ($C_4H_6ClN_4^+$)($C_7H_5O_6S^-$)·H_2O (**2**), ($C_5H_8N_3^+$)($C_7H_5O_6S^-$)·H_2O (**3**), ($C_5H_7N_6^+$)($C_7H_5O_6S^-$)·H_2O (**4**), ($C_6H_{14}N_2^{2+}$)($C_7H_4O_6S^{2-}$)·H_2O (**5**), and ($C_{14}H_{19}N_2^+$)($C_7H_5O_6S^-$) (**6**) have been successfully synthesized. Their crystal structures have been determined by single-crystal X-ray diffraction. Overall, compounds adopt a layered structure with aminium cations and 5-sulfosalicylic anions linked via water molecules. The solid-state architectures of these compounds are dominated by O(N,H)-H···O and N-H···N hydrogen bonds and stabilized by weak interconnects. C-Cl···π and S-O···π interactions, apart from π···π and C-H(O)···π, were reported. Diverse approaches were used to study the effect of substituents in the polyamines in solid-state arrangement. A Hirshfeld surface analysis, with associated 3D Hirshfeld surface maps and 2D fingerprint plots, molecular electrostatic potential, and energy frameworks were used to comprehensively investigate the nature and hierarchy of non-covalent interactions and inspect supramolecular differences. The contact enrichment ratio calculations provided deeper insight into the propensity of interconnects to influence crystal packing. The evaluation of the effects of H-bonding synthons resulting from different substituents in the polyamines on self-assemblies is also presented. In the context of crystal engineering, a specific intramolecular synthon via O-H···O observed in nearly all crystals can be employed in the pseudo-cyclic replacement strategy in the design of new molecules.

Keywords: 5-sulfolsalicylic acid; heterocyclic polyamines; synthesis; crystal structure; Hirshfeld surface; enrichment ratio; energy frameworks; molecular electrostatic potential

Citation: Bojarska, J.; Łyczko, K.; Mieczkowski, A. Novel Salts of Heterocyclic Polyamines and 5-Sulfosalicylic Acid: Synthesis, Crystal Structure, and Hierarchical Supramolecular Interactions. *Crystals* **2024**, *14*, 497. https://doi.org/10.3390/cryst14060497

Academic Editor: Alexander Y. Nazarenko

Received: 26 April 2024
Revised: 10 May 2024
Accepted: 20 May 2024
Published: 24 May 2024

1. Introduction

Organic salts based on 2-hydroxy-5-sulfobenzoic (5-sulfosalicylic) acid are eagerly studied due to their interesting optical and pharmaceutical properties [1–6]. Many salts, including one negative 3-carboxy-4-hydroxybenzenesulfonate anion, $C_7H_5O_6S^-$ (with a negative charge at the sulfonyl group), have been presented. These include compounds mostly with organic [7–10] but also inorganic cations [11,12]. Still, there are only a few of its salts with cations originating from pyrimidine. One salt with 2-aminopyrimidin-1-ium ion [13] and two with 2,4-diaminopyrimidin-1-ium ion derivatives can be distinguished. Among these 2,4-diaminopyrimidin-1-ium ions, the first has the trimethoxybenzyl group in the 5-position of the pyrimidine ring [14], and the second *o*-chlorophenyl and ethyl groups in the 5- and 6-positions, respectively [15]. The 2,4-diaminopyrimidin-1-ium cation has been reported in several ion pairs with simple inorganic [16] and some organic anions [17–21]. The crystal structures of a series of 2,4-diaminopyrimidin-1-ium salts with chain dicarboxylate ions have been discussed by us recently [22].

Of the presented organic connections, only the crystal structure of salt **3**, derived from 5-sulfosalicylic acid and 2,6-diaminopyridine, has been measured at room temperature earlier [23]. In addition, the crystal structure of the $C_7H_5O_6S^-$ and 2,3-diaminopyridinium ion pair has also been reported [24]. Moreover, a few other structures with 2-aminopyridinium ion [13] and its derivatives substituted by chloro [25,26], bromo [27] or methyl [28] group can be found in the CSD. For 2,6-diamino-9*H*-purin-1-ium cation, only its salts with 2-(2-carboxylatophenyl)acetate and *closo*-dodecafluorododecaborate ($B_{12}F_{12}^{2-}$) anions have been described [29,30]. In turn, for 3-carboxy-4-hydroxybenzenesulfonate anion, its salts with 9*H*-purin-6-aminium, 6-aminopurin-1-ium and 6-(benzylamino)-9*H*-purin-1-ium cations have been reported [31,32]. The ion pairs of 8-(dimethylamino)-*N*,*N*-dimethylnaphthalen-1-aminium ($dmanH^+$) and the salicylic acid derivatives have also been discussed [33,34].

Recently, salts of the dipositive 1,4-diazabicyclo[2.2.2]octane-1,4-diium cation ($dabcoH_2^{2+}$) have been widely presented as attractive materials for use in opto-electronics [35–40]. In addition, crystal structures containing 3-carboxylato-4-hydroxybenzenesulfonate dianion, $C_7H_4O_6S^{2-}$ (with a negative charge at both sulfonyl and carboxyl groups), and singly or doubly charged organic cations have been structurally characterized [1,41–44]. Among them, the salts of $C_7H_4O_6S^{2-}$ with 2-aminopyridinium [45], 2,6-diaminopyridinium [46] 2-amino-4,6-dimethylpyrimidinium [47], and 6-(benzylamino)-3*H*-purin-7-ium ions [48] can also be distinguished.

N-rich heterocyclic polyamines, together with popular multifunctional 5-sulfosalicylic acid, have received a lot of interest in both academic and industrial studies and applications as building blocks of appealing multifunctional supramolecular architectures. Supramolecular chemistry, as a key branch of crystal engineering, has wide implications in the rational design of novel compounds, especially in the context of control of the self-organization and, in further consequence, predictable and desirable structural complex assemblies (such as salts or co-crystals). H-bonding, as well as other non-covalent interactions, have emerged to be the most important tool in crystal engineering [49–51]. Organic crystals composed of specific functional groups with diverse applications attracted much attention in the context of the predictable assemblies of supramolecular architectures. The utilization of self-assembly of small compounds with either strong O(N)-H$\cdots$O or weak C-H$\cdots$O hydrogen bonds, halogen bonds, and π-based interactions to the formation and stabilization of 3D supramolecular networks is a vital aspect. The rational design of well-defined structures from complex multifunctional moieties is possible via supramolecular synthons—structural units within crystals composed of hydrogen bonds and/or other non-covalent interactions [52]. The synthons can be classified as homo- or heterosynthons, which are formed from self-complementary half units and different components/functionalities, respectively [53].

Considering all these points in the course of our supramolecular studies on the hierarchy of non-covalent interactions [22,54–57] here, we report the synthesis and thorough supramolecular investigations of the series of new salts, namely, 2,4-diaminopyrimidin-1-ium 3-carboxy-4-hydroxybenzenesulfonate dihydrate (**1**), 2,4-diamino-6-chloropyrimidin-1-ium 3-carboxy-4-hydroxybenzenesulfonate monohydrate (**2**), 2,6-diaminopyridin-1-ium 3-carboxy-4-hydroxybenzenesulfonate monohydrate (**3**), 2,6-diamino-9*H*-purin-1-ium 3-carboxy-4-hydroxybenzenesulfonate monohydrate (**4**), 1,4-diazabicyclo[2.2.2]octane-1,4-diium 2-hydroxy-5-sulfonatobenzoate monohydrate (**5**), and 8-(dimethylamino)-*N*,*N*-dimethylnaphthalen-1-aminium 3-carboxy-4-hydroxybenzenesulfonate (**6**) (Figure 1). It should be mentioned that these structures have not previously been structurally authenticated. They are presented for the first time to the best of our knowledge; only one salt (**3**) is a better re-determination, at low temperatures with a higher precision, of previously published structure (CSD refcode: KAXAE) [23]. These compounds can construct appealing supermolecules and diverse either strong or weak synthons because of the presence of a large amount of oxygen and nitrogen atoms, excellent acceptors and donors, and different functional groups such as the sulfonic, carboxylic, hydroxyl, amino, and methyl groups. In addition, water solvent molecules offer an enriched portfolio of H-bonding patterns. This study was undertaken to understand the nature and relevance of the hierarchy of

non-covalent interactions either between the cations or between the anions, as well as the cation–anion interplay, focusing on the effect of the H-bonding synthons on novel self-assemblies. The analysis of interaction preferences was supported by Full Interaction Maps. The supramolecular topology of H-bonding networks was examined by an extended Hirshfeld surface analysis, including the enrichment ratios, the molecular electrostatic potentials, and the energy frameworks.

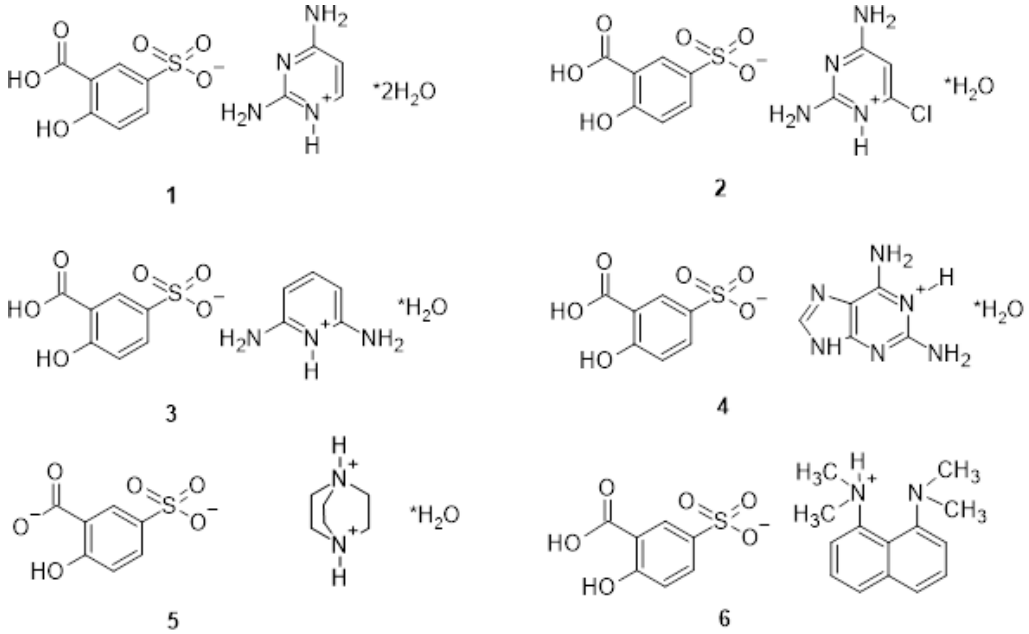

Figure 1. Structures of analysed salts: 2,4-diaminopyrimidin-1-ium 3-carboxy-4-hydroxybenzenesulfonate dihydrate (**1**), 2,4-diamino-6-chloropyrimidin-1-ium 3-carboxy-4-hydroxybenzenesulfonate monohydrate (**2**), 2,6-diaminopyridin-1-ium 3-carboxy-4-hydroxybenzenesulfonate monohydrate (**3**), 2,6-diamino-9*H*-purin-1-ium 3-carboxy-4-hydroxybenzenesulfonate monohydrate (**4**), 1,4-diazabicyclo[2.2.2]octane-1,4-diium 2-hydroxy-5-sulfonatobenzoate monohydrate (**5**), and 8-(dimethylamino)-*N*,*N*-dimethylnaphthalen-1-aminium 3-carboxy-4-hydroxybenzenesulfonate (**6**).

2. Materials and Methods

2.1. Synthesis of Compounds **1**–**6**

The commercially available chemicals were of reagent grade and used as received. The ATR-FTIR spectra were recorded on a Thermo Scientific Nicolet iS10 FTIR spectrometer using the ATR technique with ZnSe crystal. The following procedure was applied to obtain the requested crystals of heterocyclic polyamines and 5-sulfonylsalicylic acid.

The 5-sulfosalicylic acid (0.1 mmol, 1 equiv., 22 mg) and appropriate organic diamine (0.1 mmol, 1 equiv., 11 mg of 2,4-diaminopyrimidine, 15 mg of 2,4-diamino-6-chloropyrimidine, 11 mg of 2,6-diaminopyridine, 15 mg of 2,6-diaminopurine, 12 mg of 1,4-diazabicyclo[2.2.2]octane, and 22 mg of 1,8-bis(dimethylamino)naphthalene) were dissolved in 2 mL of warm distilled water, the solution was filtered through a small cotton pad and left in the room temperature for solvent evaporation (about two weeks). The obtained crystals of the salts were used for the X-ray measurements and recording the ATR-FTIR spectra.

Compound **1**: ATR-FTIR (ZnSe), ν_{max}/cm^{-1}: 3434 s, 3350 s (N–H), 3245 m (N–H), 3089 w (C–H), 3039 w (C–H), 2952 w, 2837 w, 1658 vs (C=O), 1636 m sh (C–O), 1606 sh (C–O), 1519 m, 1475 w, 1451 w, 1395 w, 1334 w (SO_3), 1295 w, 1236 sh, 1211 m sh (SO_3), 1169 s (SO_3), 1156 sh (SO_3), 1119 m, 1078 w, 1034 m, and 792 w.

Compound **2**: ATR-FTIR (ZnSe), ν_{max}/cm^{-1}: 3507 m, 3455 w (N–H), 3304 m br (N–H), 3117 s, 2772 w br, 1665 vs (C=O), 1652 sh (C=O), 1605 m (C–O), 1551 m (C–O), 1530 w,

1479 w, 1371 w (SO_3), 1305 w, 1217 m (SO_3), 1169 s (SO3), 1151 s (SO_3), 1126 s, 1079 m, 1032 s, 987 m, 796 w, 711 w, and 664 w.

Compound **3**: ATR-FTIR (ZnSe), ν_{max}/cm^{-1}: 3471 m, 3424 m, 3372 m (N–H), 3343 (N–H), 3271 m, 3221 m, 3124 w, 3096 w (C–H), 3075 w (C–H), 2974 w br, 2863 m br, 2790 m br, 2703 w br, 1652 vs (C=O), 1631 s (C=O), 1582 m (C–O), 1474 w, 1432 w, 1406 w, 1303 w (SO_3), 1225 m (SO_3), 1208 m (SO_3), 1169 m sh (SO_3), 1158 m (SO_3), 1144 m, 1116 s, 1017 s, 922 w, 830 w, 775 w, 714 w, and 662 w.

Compound **4**: ATR-FTIR (ZnSe), ν_{max}/cm^{-1}: 3397 vs br, 3360 vs br (N–H), 3209 vs br (N–H), 3048 m (C–H), 2851 w br, 1655 s sh (C=O), 1619 s (C=O), 1588 s sh (C–O), 1478 m, 1437 m, 1406 w, 1377 w (SO_3), 1347 w sh, 1156 m (SO_3), 1125 m (SO_3), 1086 w, 1029 w, and 668 w.

Compound **5**: ATR-FTIR (ZnSe), ν_{max}/cm^{-1}: 3394 w br (N–H), 3045 w (C–H), 2566 w vbr, 1644 w (C=O), 1595 m (C–O), 1474 m, 1377 w (SO_3), 1291 w, 1270 w, 1291 s (SO_3), 1180 s (SO_3), 1159 m (SO_3), 1145 s (SO_3), 1122 s, 1084 m, 1076 m, 1057 w, 1034 s, 1021 vs, 888 w br, 832 m, 777 w br, 728 w, and 668 s.

Compound **6**: ATR-FTIR (ZnSe), ν_{max}/cm^{-1}: 3050 w (C–H), 3004 w (C–H), 2973 w, 1662 m (C=O), 1603 m (C–O), 1585 w, 1474 m, 1465 m, 1288 w, 1250 s (SO_3), 1216 s (SO_3), 1188 w, 1157 m (SO_3), 1140 s (SO_3), 1119 m, 1080 m, 1016 vs, 885 w, 841 m, 831 m, 784 w, 767 m, 746 w br, 711 m, and 664 m.

2.2. Single-Crystal X-ray Diffraction

Diffraction data of single crystals of the studied compounds were collected at T = 100 K using a mirror-monochromated Cu Kα radiation (λ = 1.54184 Å) from a microfocus Nova X-ray source on a Rigaku SuperNova (dual source) four-circle diffractometer operating with an Eos CCD detector. CrysAlis PRO software (version CrysAlisPro 1.171.41.112a) was used to perform data collection and reduction, and multi-scan absorption correction. Direct method and full matrix least-squares treatment on F^2 data were applied to solve and refine the crystal structures. All non-hydrogen atoms were refined with anisotropic atomic displacement parameters. Hydrogen atoms bonded to carbon atoms were placed in calculated positions and refined isotropically as a riding model with standard parameters. The H atoms bonded to the N and O atoms were located from a different Fourier map, and their positions were freely refined. All calculation procedures were carried out using SHELXTL programs [58], integrated with the OLEX2 crystallographic software (version 1.3) [59]. Mercury (version 2023.3.1) [60] and PLATON (version 2023.1) [61] programs were applied for the graphical representation of the structures and geometry analysis.

2.3. Computational Details

2.3.1. Full Interaction Maps

3D Full Interaction Maps (FIMs) based on CSD interaction data [62] for all analyzed crystals to check their preferred interaction behavior were calculated using Mercury software [60]. This tool generates the landscape of interactions using 3D coordinates from an X-ray experiment. The comparison of the predicted most likely positions of functional groups with a crystal packing can help evaluate whether a corresponding crystal fulfills the desired interactions.

2.3.2. Hirshfeld Surface Analysis

A Hirshfeld analysis was performed using the newest version of CrystalExplorer 21.5 [63,64]. The 3D maps of the Hirshfeld's surfaces revealing qualitative information on non-covalent interactions were mainly mapped with the d_{norm} property by a colored scheme, where red spots denote the shortest inter-contacts, the white regions illustrate distances close to the van der Waals (vdW) contacts (d_{norm} equal to zero), and the blue areas signify the interactions longer than the sum of the vdW radii (positive values of d_{norm}) [64]. The map was generated by calculation of the normalized distances from the contact points on the surface to the nearest nucleus inside (d_i) or outside (d_e) the Hirshfeld surface

where all H-bond lengths adopted the neutron-derived values [65]. Two-dimensional fingerprint plots, drawn as a function of d_i and d_e values, reveal quantitative data on close inter-contacts [64].

2.3.3. Molecular Electrostatic Potential

The molecular electrostatic potential mapped onto Hirshfeld surfaces was obtained at the wave function of the HF/STO-3G level using Crystal Explorer 21.5 [63,66].

2.3.4. The Enrichment Ratio

The enrichment ratios (ER) of the intermolecular interactions in the analyzed crystal structures **1**–**6** were calculated based on the HS methodology. ER for an element pair (X, Y) is the ratio of the actual percentage of random inter-contacts within the crystal (CXY) to the percentage of theoretically equivalently distributed random contacts (RXY), when EXY = CXY/RXY. In this way privileged (when ER > 1) and disfavored inter-contacts (ER < 1) can be highlighted in the crystal structures [67].

2.3.5. Energy Frameworks

The pairwise interaction energies between the moieties within the crystal were computed by Crystal Explorer 21.5 program [63,64,66,68,69] using the wavefunction calculated at the B3LYP/6-31G(d,p) functional basis set that is widely accepted in computational chemistry. The electrostatic (E_{ele}), polarization (E_{pol}), dispersion (E_{disp}), and exchange repulsion (E_{rep}) energy components, according to Equation (1), were obtained. More specifically, the electrostatic term is characterized by the forces among charged particles, the polarization term is concerned with the interactions resulting from the distortion of a molecule's electron cloud via other near-charge distributions, dispersion term is considered to be the weak forces caused by fluctuations in a molecule's electron distribution, while repulsion term means the energy needed to overcome the forces that prevent a molecules pair from interaction [70,71].

To calculate the total energy (E_{tot}) framework, a molecular cluster with a radius of 3.8 Å was generated around a selected single moiety of the reference compound. Symmetry operations were applied to build molecular wave functions and calculate the electron densities of a cluster. A tube size of 100 was used for the images.

$$E_{tot} = E_{ele} + E_{pol} + E_{disp} + E_{rep} \quad (1)$$

3. Results and Discussion

3.1. X-ray Structure and Supramolecular Features

The crystal structures of **1**–**6** were determined by single crystal X-ray diffraction with high precision at low temperature. Crystals **1**, **2**, **4**, **5**, and **6** are novel, while **3** is a better equivalent of the previously published structure KASXAE, which was earlier determined at ambient temperature [23]. The molecular structures of **1**–**6** are shown in Figure 2. Compounds **1**, **2**, **4**, and **5** crystallize in the triclinic $P\bar{1}$ space group, while compounds 3 and **6** crystallize in the monoclinic space groups—$P2_1$ and $P2_1/c$, respectively. Full crystallographic data of studied salts are collected in Table 1. The unit cells of **1**–**5** contain solvent (water) molecules, apart from aminium cation and 5-sulfosalicylate anion. The unit cell of **6** consists of two crystallographically independent cations and anions. The structure of **5** represents the dicationic and dianionic species. The deprotonated carboxylic (COO^-) and sulfonic (SOO^-) groups of the anion show bond lengths of 1.275 and 1.261, as well as 1.453 and 1.456 Å, respectively. It indicates a delocalized anionic charge. Selected bond lengths and angles of **1**–**6** can be found in Table S1. The values are comparable to those found in the literature.

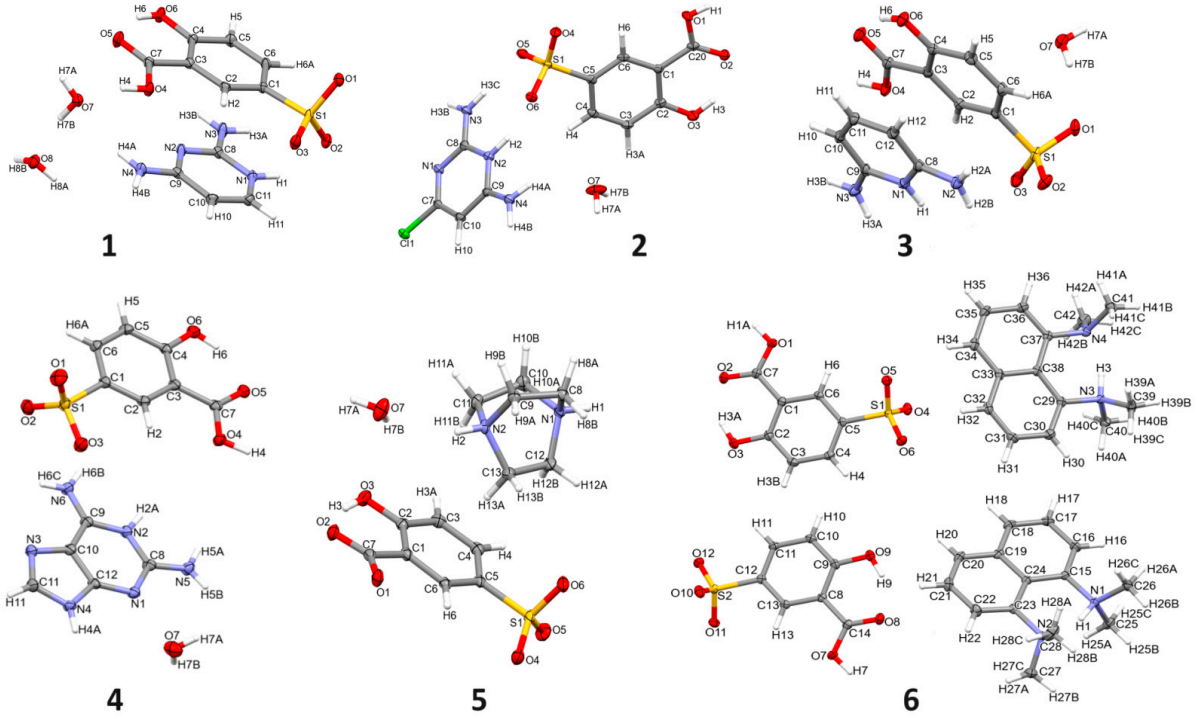

Figure 2. The molecular structures of **1**–**6** showing the atom numbering schemes. Displacement ellipsoids are drawn at a 30% probability level.

Table 1. Crystal data and structure refinement details obtained from measurements at 100 K for the studied compounds.

Compound	1	2	3	4	5	6
Chemical formula	$C_{11}H_{16}N_4O_8S$	$C_{11}H_{13}ClN_4O_7S$	$C_{12}H_{15}N_3O_7S$	$C_{12}H_{14}N_6O_7S$	$C_{13}H_{20}N_2O_7S$	$C_{21}H_{24}N_2O_6S$
Formula weight	364.34	380.76	345.33	386.35	348.37	432.48
λ (Cu Kα) (Å)	1.54184	1.54184	154184	1.54184	1.54184	1.54184
Crystal system	triclinic	triclinic	monoclinic	triclinic	triclinic	monoclinic
Space group	$P\bar{1}$	$P\bar{1}$	$P\,2_1$	$P\bar{1}$	$P\bar{1}$	$P\,2_1/c$
a (Å)	7.9539(3)	6.8906(6)	6.6358(2)	6.6755(4)	6.7903(4)	19.7312(3)
b (Å)	9.5529(4)	6.9077(6)	12.9481(4)	10.6495(5)	8.7284(8)	12.33559(11)
c (Å)	11.2394(4)	16.9140(11)	8.4812(3)	10.9153(5)	13.3336(7)	18.4437(3)
α (°)	67.904(4)	96.621(6)	90	84.427(4)	101.707(6)	90
β (°)	85.375(3)	96.880(6)	104.703(3)	87.076(5)	103.408(5)	114.7954(16)
γ (°)	78.700(3)	108.636(8)	90	83.698(5)	94.585(6)	90
Volume (Å)	775.92(6)	747.20(11)	704.84(4)	767.01(7)	746.02(9)	4075.28(10)
Z	2	2	2	2	2	8
D_{calc} (g·cm^{-3})	1.559	1.692	1.627	1.673	1.551	1.775
μ (mm^{-1})	2.344	4.022	2.470	2.405	2.312	1.410
F (000)	380	392	360	400	368	1824
Crystal size (mm)	0.18 × 0.16 × 0.08	0.15 × 0.08 × 0.03	0.18 × 0.10 × 0.05	0.22 × 0.04 × 0.03	0.18 × 0.14 × 0.10	0.20 × 0.18 × 0.10
θ range (°)	4.245–70.422	2.667–70.282	5.392–70.328	4.073–70.352	3.500–70.225	2.467–70.187
Reflections collected	11,295	5414	4501	9276	4728	28,523
Unique reflections	2926	2792	2451	2858	2776	7674
Reflections $I > 2\sigma(I)$	2805	2419	2365	2484	2513	6949
R_{int}	0.0220	0.0290	0.0211	0.0361	0.0187	0.0222
Restraints/parameters	1/261	1/253	1/244	0/274	1/223	2/567
Goodness-of-fit	1.086	1.116	1.073	1.073	1.047	1.043
R_1, wR_2 ($I > 2\sigma(I)$)	0.0261, 0.0735	0.0379, 0.0986	0.0276, 0.0695	0.0432, 0.1096	0.0335, 0.0853	0.0303, 0.0827
R_1, wR_2 (all data)	0.0273, 0.0745	0.0443, 0.1047	0.0293, 0.0716	0.0533, 0.1161	0.0373, 0.0881	0.0338, 0.0855
Max. peak/hole (e·Å^{-3})	0.359/−0.468	0.307/−0.602	0.202/−0.298	0.674/−0.473	0.398/−0.427	0.302/−0.482
K.P.I. [%]	70.2	72.6	72.7	74.2	70.6	74.4

K.P.I.—Kitaigorodsky's packing index.

The crystal packing can be quantified by the Kitaigorodsky packing index (K.P.I.) [72,73]. It was calculated with the 'calc void' procedure implemented in the PLATON program [61]. The results showed that **6** is the most, while **1** is the least closely packed structure with 74.4% and 70.2% of filled space, respectively. No space accessible for voids was found (Table 1). The appealing feature of analyzed salts is the presence of diverse functional groups (sulfonate, carboxyl, hydroxyl, amine, methyl) with available H-atom donor and acceptor atoms of both cation and anion species, as well as water molecules, which results in extensive H-bonding interactions. The crystal packing of all salts is formed mainly by O-H···O, N-H···O, and C-H···O interactions, with the distances shorter than the sum of the mean van der Waals radii of the two corresponding atoms, from 1.63 Å for O-H···O in **4** and **6** to 2.59 Å for C-H···O in **5**. Furthermore, O-H···N in **1** and N-H···N interactions in **2**, **4**, and **6** are observed. The intramolecular network is affected by O-H···O and C-H···O, and also N-H···N in **6**. The geometrical parameters of H-bonds are listed in Table 2. It can be mentioned that nearly all available acceptors in all crystals, apart from **6**, interact with all available donors. The two oxygen atoms in the sulfonic group play the role of bifurcated acceptors participating in the formation of O(N,C)-H···O interactions with anion, cation, and water molecules. A rare trifurcated (and tetrafurcated) acceptor is observed in **6** (Figures 3–8).

Table 2. Geometric parameters of H-bonds for **1**–**6**.

9	**D-H [Å]**	**H···A [Å]**	**D···A [Å]**	**D-H···A [º]**
1				
N1-H1···O2 ^{i}	0.883(19)	1.869(19)	2.7472(14)	172.7(17)
N3-H3A···O8 ^{ii}	0.886(19)	2.154(19)	2.9655(16)	152.1(17)
N3-H3B···O5 ^{iii}	0.853(19)	2.136(19)	2.9698(16)	165.5(19)
O4-H4···O7	0.90(2)	1.69(2)	2.5685(13)	166(3)
N4-H4A···O6 ^{ii}	0.857(19)	2.141(19)	2.9205(17)	151.1(17)
N4-H4B···O3 ^{iv}	0.869(19)	2.082(19)	2.9313(16)	165.5(18)
*O6-H6···O5	0.86(2)	1.87(2)	2.6397(14)	149(2)
O6-H6···N2 ^{iii}	0.86(2)	2.44(2)	2.9052(15)	114.9(17)
O7-H7A···O1 ^{v}	0.83(2)	1.96(2)	2.7803(14)	172(2)
O7-H7B···O8	0.84(2)	1.90(2)	2.7306(15)	168(2)
O8-H8A···O3 ^{iv}	0.81(2)	2.10(2)	2.8640(14)	157(2)
O8-H8B···O1 ^{vi}	0.85(3)	1.93(3)	2.7594(15)	166(2)
*C2-H2···O3	0.95	2.53	2.9197(17)	105
C5-H5···O1 ^{vii}	0.95	2.57	3.2961(16)	134
C10-H10···O4 ^{iv}	0.95	2.54	3.2942(18)	137
C11-H11···O7 ^{iv}	0.95	2.42	3.3590(18)	168
(i) $1-x, 1-y, 2-z$; (ii) $x, y, 1+z$; (iii) $-x, 2-y, 1-z$; (iv) $1-x, 1-y, 1-z$; (v) $-x, 1-y, 1-z$; (vi) $x, 1+y, -1+z$; (vii) $-x, 1-y, 2-z$				
2				
O1-H1···O4 ^{i}	0.80(3)	1.93(3)	2.666(3)	154(3)
N2-H2···O6	0.94(4)	1.84(4)	2.758(3)	166(3)
*O3-H3···O2	0.89(4)	1.85(4)	2.615(3)	144(3)
N3-H3B···N1 ^{ii}	0.87(3)	2.10(3)	2.953(3)	170(3)
N3-H3C···O5	0.89(4)	1.98(3)	2.862(3)	169(3)
N4-H4A···O2 ^{iii}	0.86(3)	2.08(3)	2.925(3)	168(3)
N4-H4B···O7	0.92(4)	1.92(4)	2.813(3)	163(3)
O7-H7A···O5 ^{iv}	0.82(3)	2.02(3)	2.838(3)	174(3)
O7-H7B···O6 ^{v}	0.78(5)	2.11(5)	2.867(3)	164(5)
C3-H3A···O3 ^{vi}	0.95	2.54	3.355(4)	144
*C6-H6···O4	0.95	2.48	2.885(3)	106
C6-H6···O1 ^{i}	0.95	2.54	3.339(3)	142
(i) $3-x, 1-y, 1-z$; (ii) $1-x, -y, -z$; (iii) $2-x, 1-y, 1-z$; (iv) $-1+x, 1+y, z$; (v) $-1+x, y, z$; (vi) $1-x, -y, 1-z$				
3				
N1-H1···O7	0.86(4)	1.91(4)	2.754(4)	170(4)

Table 2. *Cont.*

9	**D-H [Å]**	**H···A [Å]**	**D···A [Å]**	**D-H···A [º]**
N2-H2A···O3 [i]	0.85(5)	2.38(5)	3.206(3)	163(4)
N3-H3A···O6 [ii]	0.85(5)	2.24(5)	3.012(3)	152(4)
N3-H3B···O2 [iii]	0.87(4)	2.09(4)	2.924(3)	162(4)
O4-H4···O1 [iii]	0.88(4)	1.76(4)	2.613(2)	165(4)
*O6-H6···O5	0.80(5)	1.89(5)	2.606(3)	148(5)
O7-H7A···O3	0.81(5)	2.07(5)	2.842(4)	161(5)
O7-H7B···O1 [iv]	0.81(5)	2.00(5)	2.768(3)	160(5)
*C2-H2···O3	0.95	2.53	2.917(4)	104
(i) $1-x, -1/2+y, 2-z$; (ii) $1-x, ½+y, 1-z$; (iii) $x, y, -1+z$; (iv) $1+x, y, z$				
4				
N2-H2A···O7	0.91(3)	1.84(3)	2.730(3)	166(3)
O4-H4···N3 [i]	0.97(4)	1.63(4)	2.573(2)	165(4)
N4-H4A···N1 [ii]	0.87(3)	2.04(3)	2.891(3)	170(3)
N5-H5A···O7	0.88(3)	2.36(3)	3.091(3)	141(3)
N5-H5B···O2 [iii]	0.84(3)	1.99(3)	2.817(3)	170(3)
*O6-H6···O5	0.86(3)	1.82(3)	2.594(2)	150(3)
N6-H6B···O3	0.89(3)	1.94(3)	2.781(3)	159(2)
N6-H6C···O5 [iv]	0.84(3)	2.02(3)	2.851(3)	168(3)
O7-H7A···O1 [v]	0.83(4)	2.07(4)	2.827(3)	153(4)
O7-H7B···O3 [vi]	0.80(4)	2.09(4)	2.877(3)	165(3)
*C2-H2···O3	0.95	2.47	2.868(3)	105
C5-H5···O6 [vii]	0.95	2.58	3.455(3)	153
C11-H11···O2 [viii]	0.95	2.37	3.098(3)	133
(i) x, $1+y, z$; (ii) $1-x, -y, 2-z$; (iii) $x, y, 1+z$; (iv) $x, -1+y, z$; (v) $-x, 1-y, 1-z$; (vi) $1-x, 1-y, 1-z$; (vii) $-x, 2-y, -z$; (viii) $1-x, -y, 1-z$				
5				
N1-H1···O6 [i]	0.91(2)	1.84(2)	2.7102(18)	161(2)
N2-H2···O1 [ii]	0.916(17)	1.632(17)	2.5451(18)	174.0(17)
N2-H2···O2 [ii]	0.916(17)	2.59(2)	3.1463(19)	119.9(14)
*O3-H3···O2	0.91(3)	1.67(3)	2.5278(19)	155(2)
O7-H7A···O4 [iii]	0.85(3)	2.13(2)	2.9623(19)	168(2)
O7-H7B···O5 [iv]	0.81(3)	2.05(3)	2.841(2)	167(2)
*C6-H6···O4	0.95	2.59	2.951(2)	103
C8-H8A···O5 [v]	0.99	2.47	3.423(2)	161
C8-H8B···O7 [vi]	0.99	2.44	3.314(3)	147
C9-H9B···O3 [vi]	0.99	2.47	3.329(2)	145
C11-H11A···O2 [vi]	0.99	2.59	3.363(2)	135
C13-H13B···O7 [vi]	0.99	2.59	3.356(2)	134
(i) $1-x, 1-y, 2-z$; (ii) $-x, 1-y, 1-z$; (iii) $1+x, y, -1+z$; (iv) $1-x, -y, 1-z$; (v) $1+x, 1+y, z$; (vi) $1-x, 1-y, 1-z$				
6				
*N1-H1···N2	0.930(18)	1.713(18)	2.5973(15)	157.6(17)
O1-H1A···O5 [i]	0.93(2)	1.63(2)	2.5468(13)	169(2)
*N3-H3···N4	0.93(2)	1.707(19)	2.5907(16)	158.8(17)
*O3-H3A···O2	0.87(2)	1.83(2)	2.6134(17)	148(2)
O7-H7···O11 [ii]	0.92(2)	1.66(2)	2.5714(13)	169(2)
*O9-H9···O8	0.89(2)	1.79(2)	2.6005(16)	149(2)
C25-H25B···O4 [iii]	0.98	2.52	3.4370(16)	157
C25-H25C···O2 [iv]	0.98	2.51	3.3061(18)	138
C26-H26A···O5 [v]	0.98	2.46	3.3977(18)	161
C27-H27C···O10	0.98	2.57	3.381(2)	140
C30-H30···O11 [vi]	0.95	2.49	3.4349(16)	173
C39-H39C···O8 [iii]	0.98	2.51	3.0482(17)	114
C40-H40A···O10 [vi]	0.98	2.39	3.3235(18)	159
C41-H41B···O12	0.98	2.50	3.1961(17)	128
C42-H42C···O12	0.98	2.58	3.2782(16)	128
(i) $-x, ½+y, ½-z$; (ii) $1-x, -1/2+y, ½-z$; (iii) $x, -1+y, z$; (iv) $x, -1+y, z$; (v) $-x, -1/2+y, ½-z$; (vi) $1-x, 1-y, -z$				

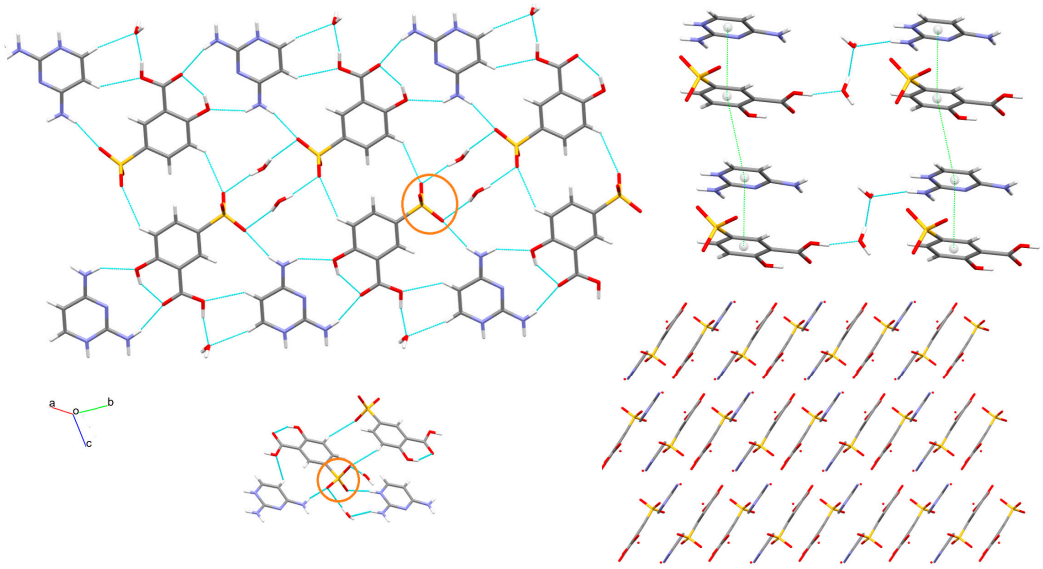

Figure 3. Crystal packing of **1**.

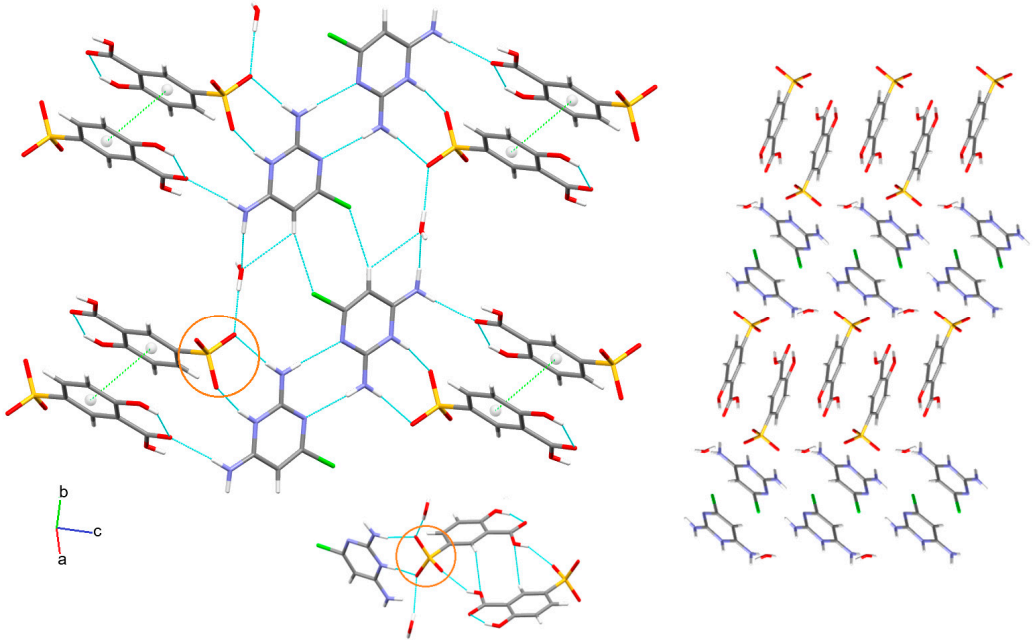

Figure 4. Crystal packing of **2**.

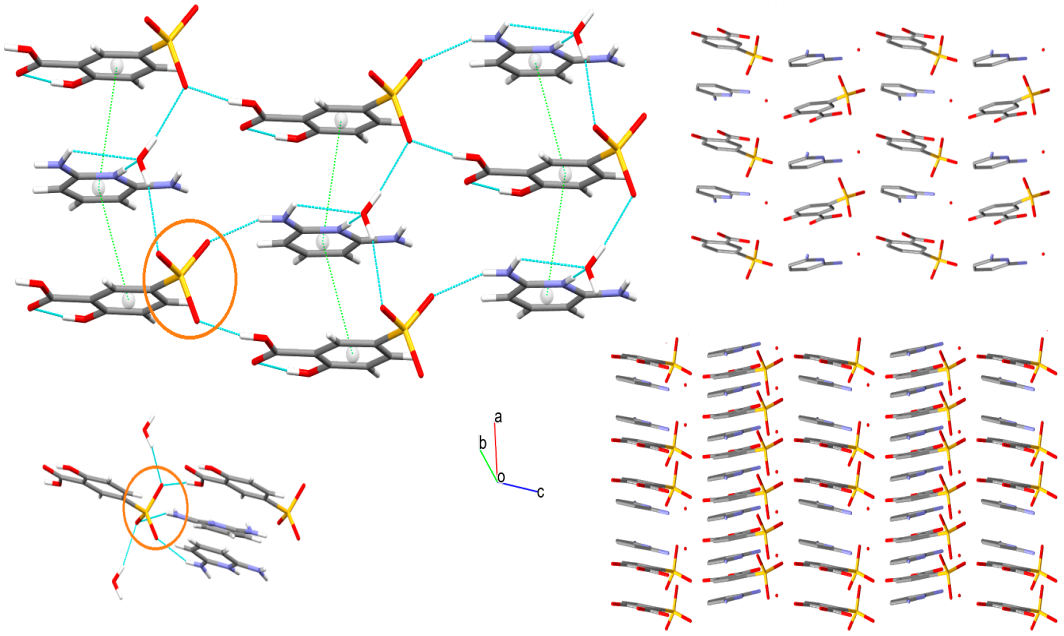

Figure 5. Crystal packing of **3**.

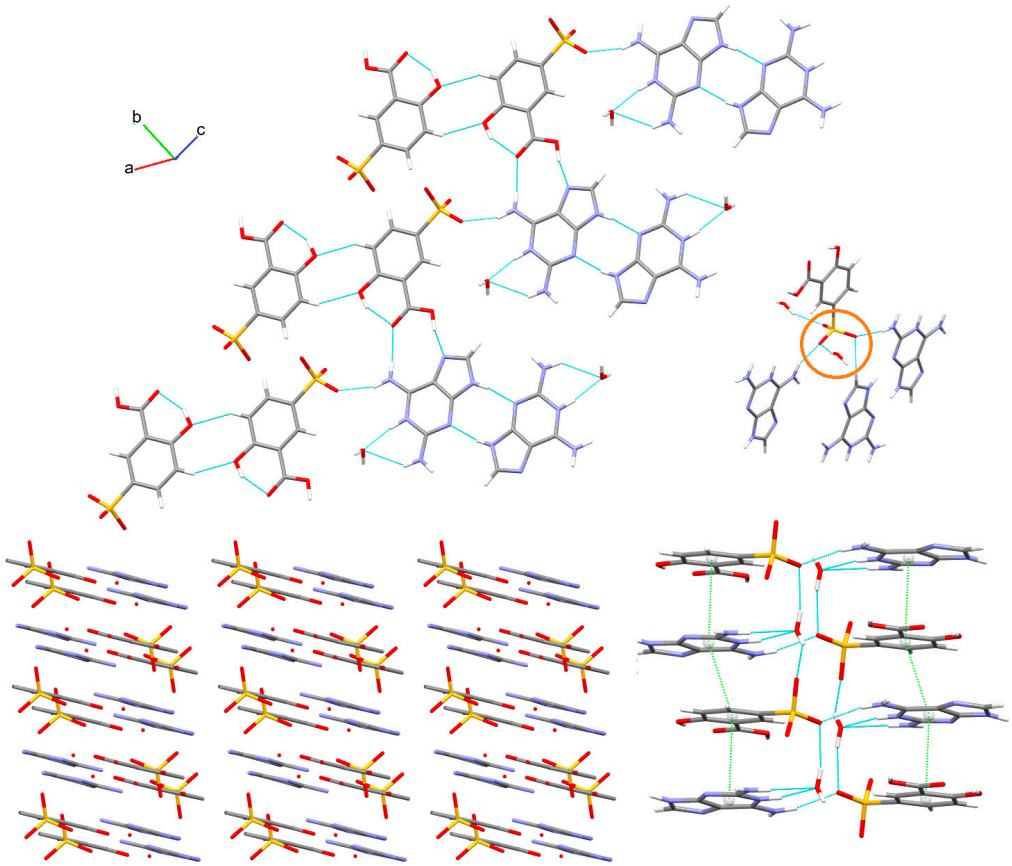

Figure 6. Crystal packing of **4**.

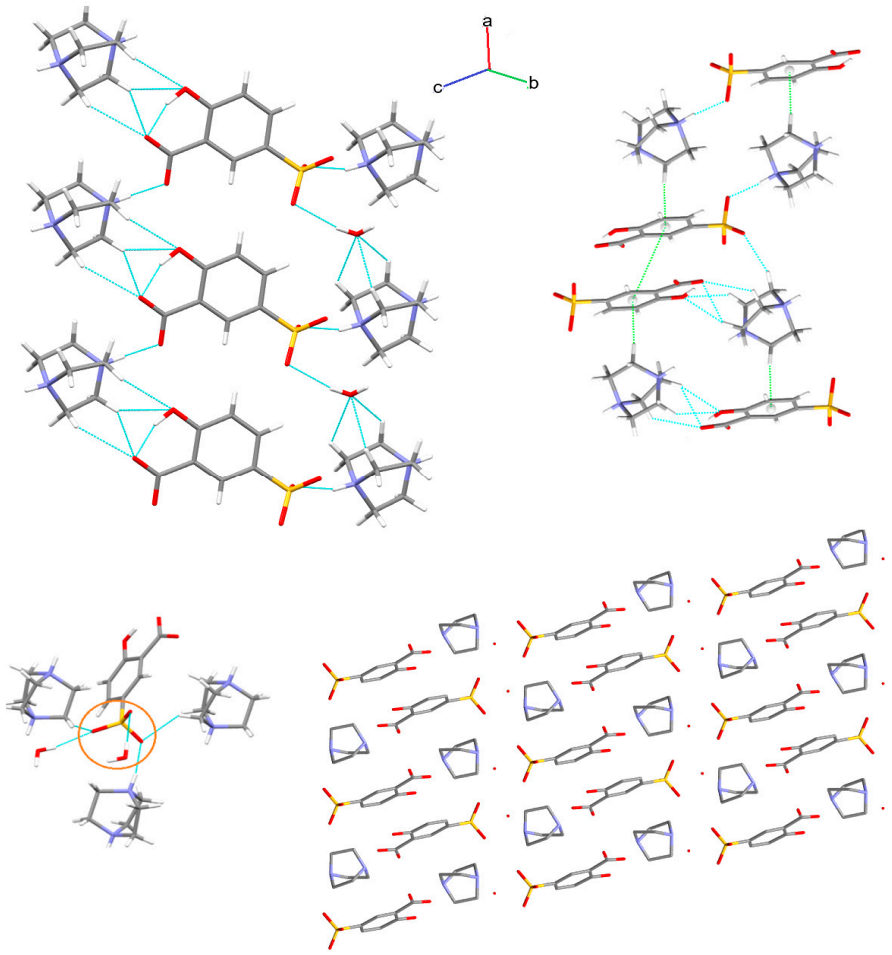

Figure 7. Crystal packing of **5**.

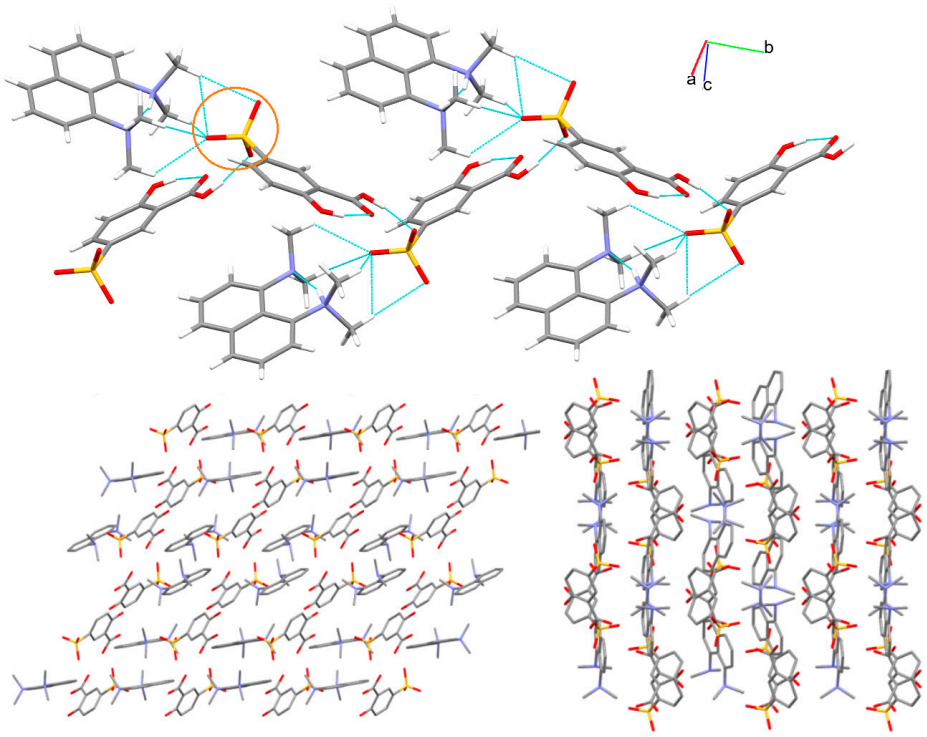

Figure 8. Crystal packing of **6**.

Overall, at first glance, novel salts exhibit similar self-assembly behavior. Nevertheless, a thorough examination revealed that the structures differ markedly as demonstrated in Figures 3–8. More specifically, compounds feature extensive H-bonding 3D-layered structures with significant π···π interactions in **2**–**4** with a Cg-Cg distance below 4 Å; and with the shortest distance—3.4111(12) Å in **4,** and C-H···π in **5** and **6** (H···Cg distance below 3 Å) between the cations and anions, as demonstrated in Figures 3–8. With respect to other weak π-based interactions, C-O···π (O···Cg distance below 4 Å) exist in **2**, **4**, and **5**. It can be noted that the S-O···π [3.841(2) Å] inter-contact and C-Cl···π [Cl-Cg distance 3.6827(13) Å] halogen interaction were found in **2** (see Tables S2 and S3). In **2**, a specific zig-zag layered structure is formed via alternating perpendicular separate anionic and cationic layers. Notably, water solvent molecules are significant contributors to building supramolecular architectures in all suitable cases (**1**–**5**). They play an important role as either a donor or acceptor of a bridge-linking moieties. The interplay of strong and weak H-bonding interactions and π-based inter-contacts gives rise to interesting supramolecular motifs at diverse levels of self-assembly. First of all, a specific intramolecular synthon, namely S(6), via O-H···O between the phenol OH group and a carboxyl O atom is observed in all crystals (Figure 9). It is key information from the crystal engineering point of view. This synthon can be employed in the pseudo-ring replacement strategy in the design of molecules. Another intramolecular H-bonding supramolecular motif via $_{(NH)}$N-H···N$_{(N)}$ interactions in cationic moiety, but denoted by a similar descriptor *S*(6), is observed in crystal **6** (Table S4). In **2** and **4**, a robust and very popular homosynthon $R^2_2(8)$ via O-H···O interaction is observed. Additionally, other centrosymmetric dimers, such as $R^2_2(16)$ in **2** by O-H···O, $R^2_2(12)$ in **1**, $R^2_2(10)$ and $R^2_2(13)$ in **2** through C-H···O, were found. Moreover, heterosynthon $R^2_2(7)$ via O-H···O and C-H···O interactions is generated. Here, the OH group plays as role of either donor or acceptor simultaneously (Table S4). Moving forward, water molecules, linking ions, are involved in the formation of cyclic homosynthons as a donor and acceptor. Figure 9 illustrates the above supramolecular motifs taking into account anions. On the other hand, the protonated pyridine N atom of a cation forms diverse, interesting H-bonding supramolecular motifs with either COOH/COO$^-$ or SO$^-$ groups of anions or the water molecules as shown in Figure S1 (in Supplementary Materials). A library of supramolecular H-bonding synthons, including the first and second levels of the graph-set theory is provided (see Table S4). It is noteworthy that novel salts demonstrate remarkably varied supramolecular features arising mainly from different cationic polyamine species and their substituents.

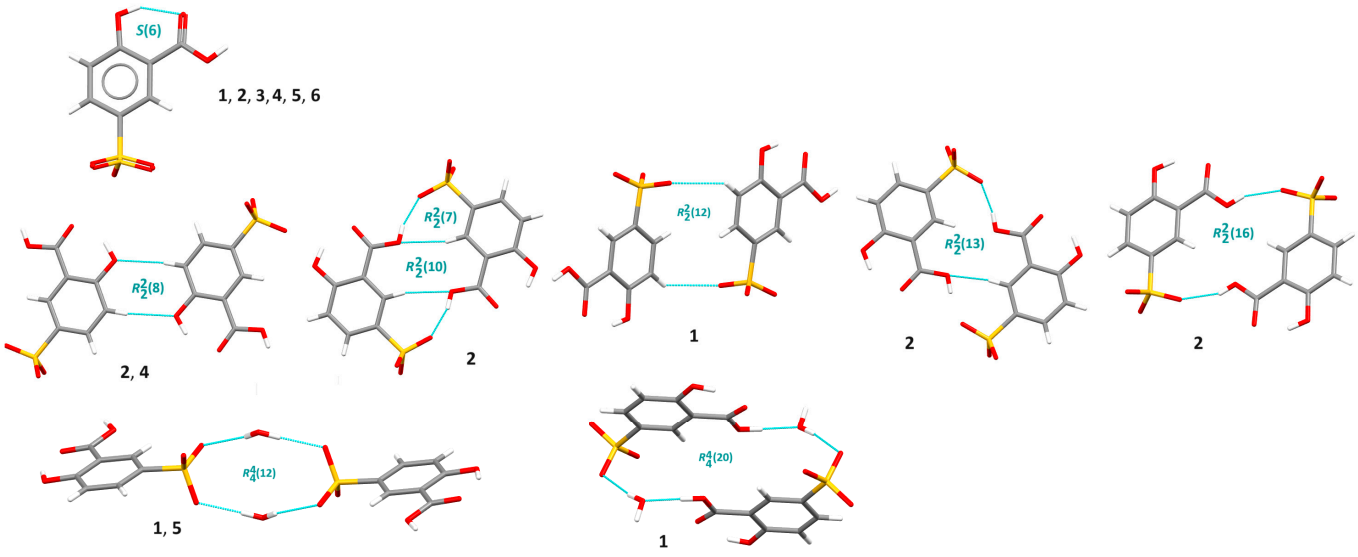

Figure 9. Supramolecular H-bonding synthonic patterns formed by anionic species in **1**–**6**.

The Full Interaction Maps (FIMs), related to statistical interaction data extracted from the CSD [62], helped us understand the effect of diverse substituents in the polyamines on supramolecular interactions and synthons formed by them. FIMs generated for all analyzed salts in the Mercury program [55] are presented in Figure 10. They illustrate zones around cations and anions where interactions are expected. It allowed us to estimate whether synthon preferences within the corresponding crystal lattices are satisfied. The FIMs of analyzed compounds **1**–**6** visualize the expected directions of the formation of either H-bonding or π-based interactions. Notably, nearly identical maps were obtained for the anions in all analyzed crystals, apart from **5**. On the other hand, FIMs for cations are completely different. Areas of H-bonding donor probabilities are shown in blue while H-bonding acceptors are demonstrated in red. Aromatic/hydrophobic interactions are denoted in beige/light brown. It can be mentioned that the intensity of the color areas is compatible with the likelihood of the relevant inter-contacts occurring. It can be seen that cation **6** has the largest probability of being involved in hydrophobic interactions, while anion **5** can participate in forming synthons as acceptors only. The substituent effect on multifaceted classical and non-classical non-covalent interactions was thoroughly examined using complex Hirshfeld surfaces analysis, described in the next section.

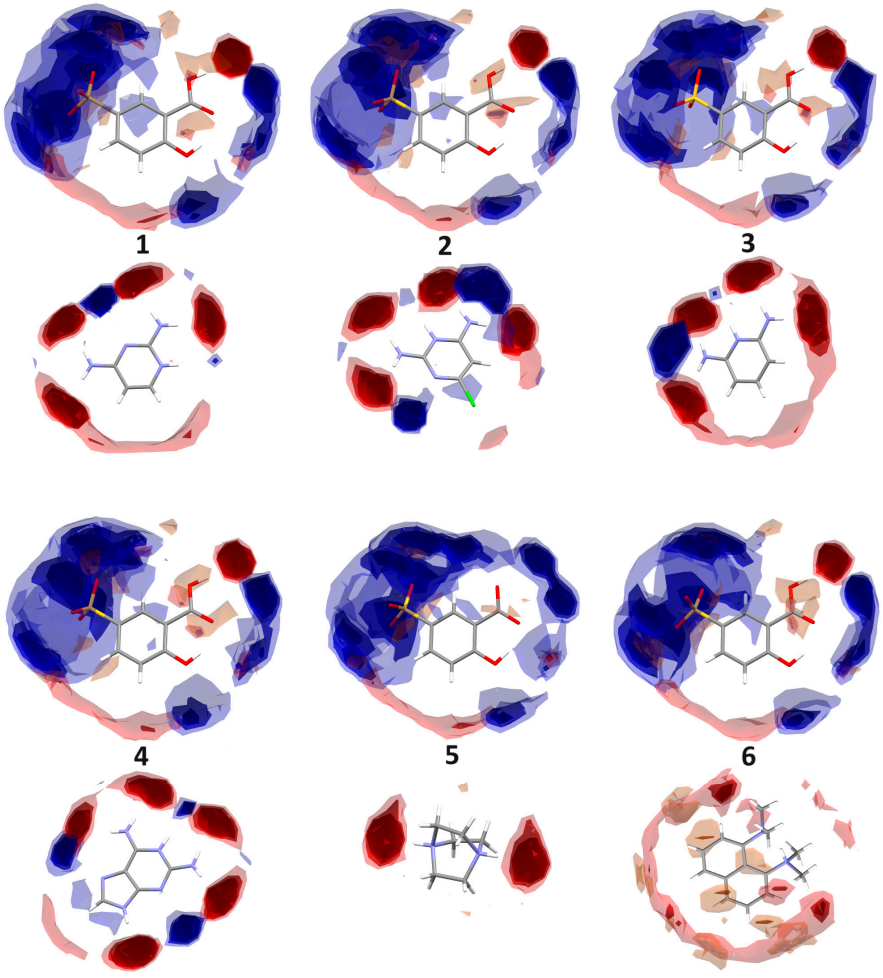

Figure 10. Full interactions maps for **1**–**6**.

3.2. Hirshfeld Surface Analysis

To gain a deep understanding of the crystal-packing behavior and the hierarchy of non-covalent interactions Hirshfeld surface analysis was performed. The 3D Hirshfeld surface maps for **1**–**6** were generated using either a standard surface solution of three-dimensional d_{norm} surfaces or shape index and curvedness properties (Figure 11). The

normalized contact distance, called d_{norm}, is the sum of the distance of the point from the nearest nucleus within the Hirshfeld surface (d_i) and the distance of the point from the nearest nucleus outside the Hirshfeld surface (d_e) normalized via the van der Waals radius of the corresponding atom [66]. The surfaces were calculated for the 5-sulfosalicylate moiety, which is the same in all compounds to emphasize nuanced differences. The bright, larger red spots on the views of the d_{norm} surfaces indicate closer distances than the van der Waals radii. In particular, they display strong H-bonding interactions such as O-H$\cdots$O and N-H$\cdots$O between carboxyl and amino groups of anions and cations, respectively. The smaller spots signify weaker C-H$\cdots$O interactions with neighboring moieties. The blue regions present longer inter-contacts than the van der Waals radii, while the white spots represent the close interactions equal to the sum of van der Waals radii. On the other hand, the convex blue spots on the shape index maps indicate hydrogen donor groups, while the concave red regions characterize acceptor groups. The $\pi\cdots\pi$ inter-contacts are represented via adjacent red and blue triangles on the shape index surfaces and as flat green areas around the rings, delineated by the blue outlines, on the curvature maps. Moving forward, orange-colored deformations of the Hirshfeld surfaces in crystals **5** and **6** indicate C-H$\cdots\pi$ interactions. For a better overview, the colored fragment patch surfaces were also generated to specify the nearest surrounding moiety [66], as shown in Figure 11. It can be used to calculate the number of moieties interacting with the main one.

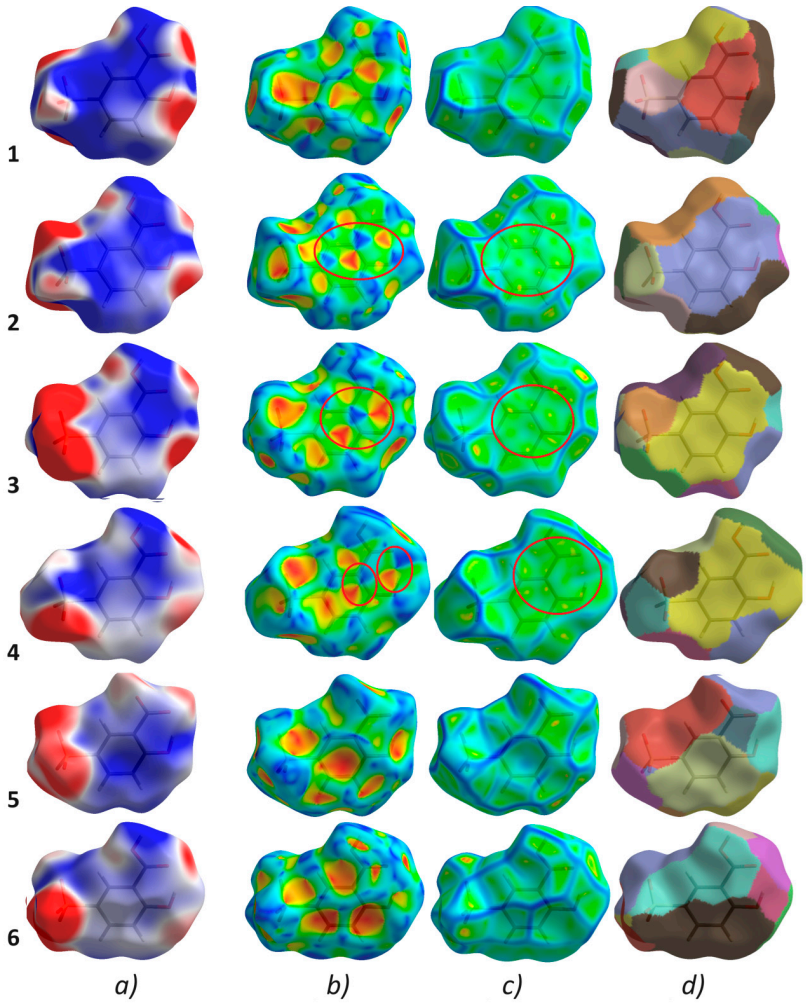

Figure 11. Views of the transparent Hirshfeld surfaces of analyzed salts **1**–**6** mapped with shape index (**b**), curvedness (**c**), and fragment patch (**d**). In addition, molecular electrostatic potential mapped on the Hirshfeld surfaces is presented (**a**). Red circles on the shape index and curvedness maps signify C$\cdots$C interactions.

3.2.1. Molecular Electrostatic Potential

In Figure 11, the electrostatic potential mapped onto the Hirshfeld surfaces is also presented. It visualizes molecular electrostatic complementarities verifying the acceptor's and donors' functions in the 3D supramolecular network. Blue areas indicate a positive electrostatic potential (H-bond donors), while red regions denote a negative electrostatic potential (acceptors) [64].

3.2.2. Fingerprints

The 2D fingerprint plots are constructed based on the distances d_e and d_i from the Hirshfeld surfaces. The shapes of the graphs are unique for each compound. They manifest differences and summarize the intricate quantitative information contained in molecular crystals **1**–**6** as illustrated in Figure 12. The percentage contribution of close interactions in these crystal structures is included in the same Figure. It is clear at first sight that the O···O/H···O interactions have the highest contribution in all crystals, at the level of 50%. They are characterized by long symmetrical/parallel 'spikes' in the fingerprint histograms. The absence of the second spike in **5** means that the anionic moiety only serves as an H-bonding acceptor, while the cationic is a donor. The H···H and C···H/H···C interactions are second and third contributors, representing an average of 21.5% and 11%, respectively. The latter interactions change from 4.9% in **2** to 23.5% in **6**. The H···H contacts are visualized in the central region between the spikes, while the C···H/H···C interactions are visualized as 'wings' in the upper side of fingerprint plots. The C···C inter-contacts are significant to share in the **2**–**4** crystal structures, showing from 3.7% in **1** to 9.8% in **2**. The C···O/O···C contacts, observed in **1**–**5**, represent from 1.5% in **3** to 8.6% in **2**. In addition, N···C/C···N contacts are observed in **1** (2.9%), **3** (3.5%), and **4** (5.3%), while N···H/H···N are reported in **1** (2.6%) and **4** (7.4%). A much smaller share falls on O···O (in **1**, **2**, and **5**) and N···O/O···N (in **1** and **4**), at a level of 3% and 1.5%, respectively (Table S5).

Enrichment ratios were calculated based on the Hirshfeld surface concept for all analyzed compounds to analyze the interactions with a high propensity to form contacts in the crystal packing. The obtained values are tabulated in Table 3 and Table S6. Privileged interactions are as follows: O···H/H···O in all crystals, C···H/H···C—in **1** and **6**, N···H/H···N in **4**, C···C in nearly all structures (apart from **6**), O···C/C···O in **2**, C···N/N···C in **1** and **4**. The highest value is obtained for the contacts O···H in **1**, C···C in **1**–**5**, and C···N in **1** and **4**. However, C···C and C···N represent only ~5.5% and 4% of the contact surfaces, respectively. Surprisingly, H···H is one of the most abundant interactions in all structures (~20%), but they are disfavored in the crystal packing. The enrichment ratio values are below 1. O···N are disfavored, while O···O are impoverished.

Table 3. Enrichment ratios for **1**–**6**.

	1	**2**	**3**	**4**	**5**	**6**
H···H	0.756	0.83	0.79	0.686	0.73	0.62
O···H	3.131	1.607	1.791	1.804	1.53	1.64
C···H	0.962	0.407	0.42	0.512	0.81	1.64
N···H	0.719			1.138		
O···O	0.246	0.247			0.27	
O···C	0.471	1.043	0.202	0.382	0.57	
O···N	0.57			0.418		
C···C	1.967	6.53	4.3	3.279	2.99	
C···N	4.03			3.223		

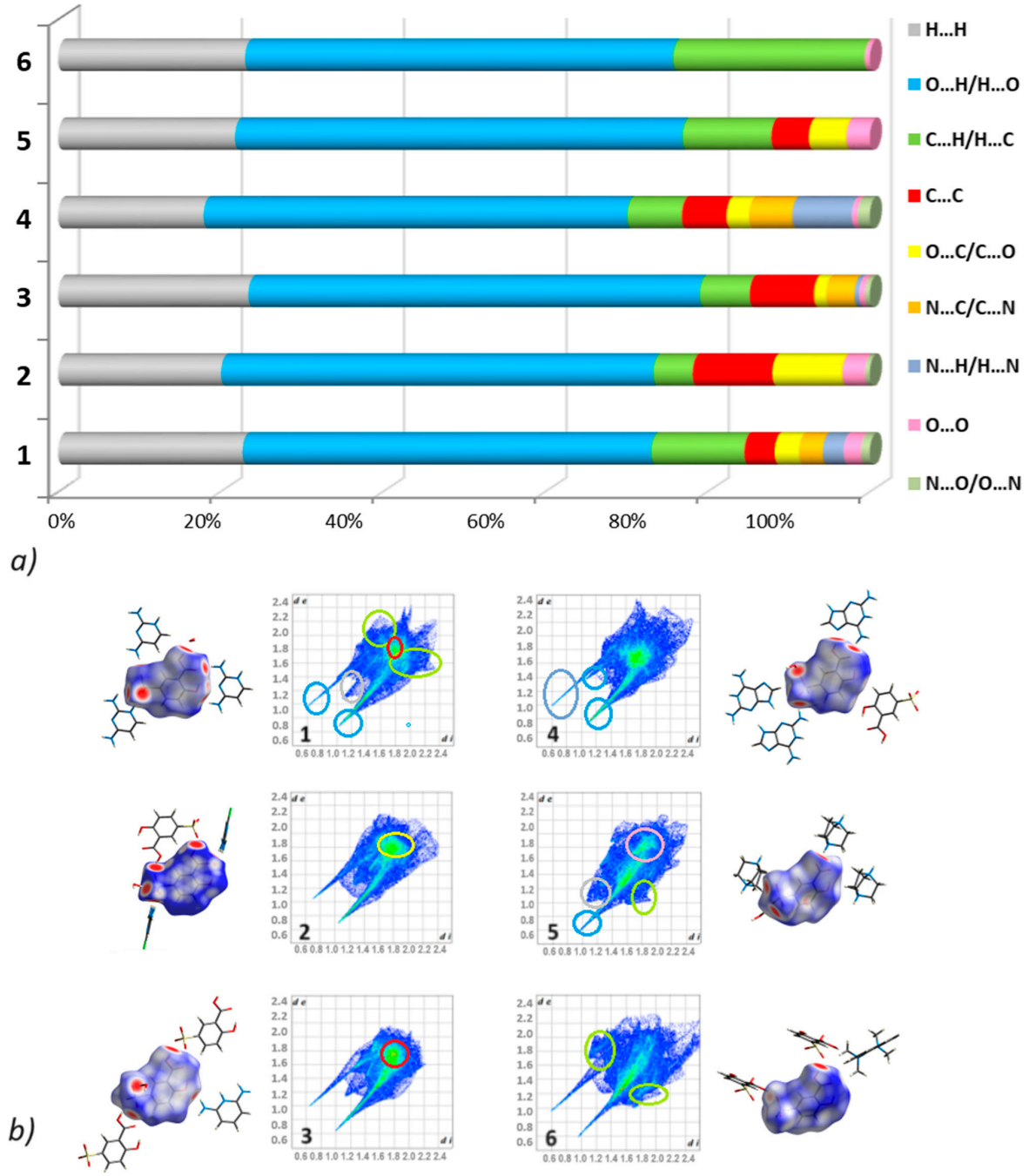

Figure 12. (**a**) Percentage contributions of individual close inter-contacts to the Hirshfeld surfaces of **1**–**6** (contacts with >0.5% are taken into account); (**b**) full fingerprint plots and Hirshfeld surfaces of the 5-sulfosalicylic moiety for **1**–**6** mapped with d_{norm} property over a range between −0.50 and 1.50 Å and drawn with the surrounding moieties. Circles on the fingerprint plots characterize corresponding interactions: C...C in red, C...H/H...C in green, H...H in blue, O...O in pink (according to the legend).

The energy framework concept enables the visualization of strong interaction chains and an understanding of the distinct energy types. The three-dimensional energy frameworks for all six analyzed compounds are depicted in Figure 13. It emphasizes the neighboring moieties located in a radius of 3.8 Å from the analyzed molecule. Energy types are symbolized by different colors. In particular, red is for classical electrostatic (the coulombic), while green is for dispersion terms. In addition, the total energy is presented in blue. Notably, the cylinder/tube size (diameter) signifies the energy value; thicker cylinders mean higher energies. The tube thicknesses denote the relative interaction strengths. The calcu-

lated values of interaction energies, including the crystallographic symmetry operations, are summarized in Table 4. It depicts the energy contributions of all components, such as electrostatic (E_{ele}), polarization (E_{pol}), dispersion (E_{disp}), and repulsion (E_{rep}), as well as total (E_{tot}) for various intermolecular interactions in the analyzed crystals. Details presented in Table 4 are pivotal for the calculations of lattice energy [71]. The results revealed several types of interactions between the center moiety and the neighboring moieties. The thorough analysis revealed that in **1**, total interaction energy (E_{tot} = −85.9 kJ/mol) is associated with a symmetric pair of molecules distanced at R = 5.66, 5.80, and 7.34 Å, respectively. Similarly, in **2**, a closer look at the obtained values of energies shows significant insights. As an example, in **1**, the electrostatic, polarization, dispersion, and repulsion energies were calculated to be −218.9, −92.5, −162.7, and 57.2 kJ/mol, respectively (see Table 4). Further analysis indicated total lattice energies: −383.5 kJ/mol for **1**, −153 kJ/mol for **2**, −469.5 kJ/mol for **3**, −237 kJ/mol for **4**, −86.8 kJ/mol for **5**, and −333.4 kJ/mol for **6**. Thus, E_{tot} values show significant differences. The most thermodynamically stable salt is considered to be **3**. Interestingly, **3** presents remarkable red cylinders that joined the molecular pairs forming a hexagon energy topology. It is noteworthy that overall, the electrostatic energy is clearly a dominant component in **1**, **3**, **4**, and **6**, while dispersive energy is in **2** and **5**. This means that van der Waals forces, contributing to dispersion interactions, are significant in the supramolecular assembly in **2** and **5**. In this regard, the interactions between the reference moiety and the symmetry-related molecule at −x, −y, and −z in **2** and **5** are the most important interactions, with E_{tot} = 175.6 and −49.7 kJ/mol, respectively.

Table 4. The interaction energies via energy framework calculations. Energy values are given in kJ mol^{-1}. (*R* means the distance between molecular centroids; *N* is the number of interactions involving the central moiety).

	N	*R*	E_{ele}	E_{pol}	E_{disp}	E_{rep}	E_{tot}	Symmetry Operation
1								
	1	5.98	7.1	0.0	−21.2	5.8	−7.1	$-x, -y, -z$
	1	5.90	7.1	−12.5	−21.2	5.8	−15.3	
	1	6.55	−66.6	0.0	−16.5	9.3	−75.2	$-x, -y, -z$
	1	5.66	−66.6	−16.4	−16.5	9.3	−85.9	
	1	7.85	15.5	−4.0	−12.9	1.3	2.6	$-x, -y, -z$
	1	7.64	−7.9	−0.7	−0.5	0.0	−9.0	
	1	5.68	−7.9	−0.7	−0.5	0.0	−9.0	
	1	5.80	−66.6	−16.4	−16.5	9.3	−85.9	
	1	3.46	9.2	−1.4	−1.4	0.0	7.2	
	1	6.38	7.1	−12.5	−21.2	5.8	−15.3	
	1	6.93	15.5	−4.0	−12.9	1.3	2.6	
	1	6.16	9.2	−1.4	−1.4	0.0	7.2	
	1	8.58	−7.4	−6.1	−3.5	0.3	−14.5	$-x, -y, -z$
	1	7.34	−66.6	−16.4	−16.5	9.3	−85.9	
			−218.9	−92.5	−162.7	57.2	−383.5	
2								
	1	5.13	28.7	−18.6	−43.8	21.2	−5.2	$-x, -y, -z$
	1	8.39	6.8	−4.2	−10.4	8.1	1.4	$-x, -y, -z$
	0	4.07	19.2	−37.6	−57.8	30.3	−32.4	$-x, -y, -z$
	1	6.89	26.6	−8.0	−10.9	2.3	13.8	x, y, z
	1	7.00	0.0	−4.2	0.0	0.0	−2.7	
	0	6.96	35.9	−2.5	−2.2	0.0	32.9	
	1	4.79	26.6	−8.0	−10.9	2.3	13.8	
	0	6.09	−176.3	−61.8	−22.7	79.7	−175.6	$-x, -y, -z$
	0	5.65	8.7	−2.3	−1.8	0.0	5.7	
	0	6.53	8.7	−2.3	−1.8	0.0	5.7	
	1	8.65	28.7	−18.6	−43.8	21.2	−5.2	
	1	7.90	28.7	−18.6	−43.8	21.2	−5.2	
			42.3	−186.7	−249.9	186.3	−153	

Table 4. *Cont.*

	N	*R*	E_{ele}	E_{pol}	E_{disp}	E_{rep}	E_{tot}	Symmetry Operation
3								
	1	9.13	8.5	−1.1	−5.6	2.9	5.2	
	1	4.05	−93.4	−30.6	−11.1	55.8	−79.8	
	1	3.65	−46.1	−18.2	−50.1	32.6	−77.5	
	2	9.01	−23.9	−3.7	−2.3	0.1	−28.7	$-x, y+1/2, z$
	2	8.48	−93.4	−30.6	−11.1	55.8	−79.8	x, y, z
	1	4.14	−12.0	−2.4	−1.9	0.0	−15.5	
	1	6.21	0.0	−0.2	0.0	0.0	−0.1	
	1	3.49	−55.6	−21.0	−48.5	28.3	−91.1	
	1	8.13	1.4	−2.5	−8.0	13.5	3.6	
	1	6.20	0.9	−8.3	−14.2	8.4	−10.4	
	2	8.49	−25.3	−5.5	−3.8	0.2	−32.6	$-x, y+1/2, z$
	1	5.82	−0.9	−5.1	−9.2	1.2	−11.5	
	1	7.81	−11.2	−8.7	−12.9	15.0	−16.5	
	1	7.58	−33.3	−14.8	−9.0	20.8	−34.8	
			−384.3	−152.7	−187.7	234.6	−469.5	
4								
	1	7.40	−76.4	−14.8	−11.5	2.8	−95.6	$-x, -y, -z$
	1	8.81	6.5	−3.1	−8.9	5.7	1.3	$-x, -y, -z$
	1	9.38	0.0	−2.4	0.0	0.0	−1.6	
	1	9.45	15.2	−2.7	−5.5	0.4	9.1	$-x, -y, -z$
	1	7.04	6.5	−3.1	−8.9	5.7	1.3	
	1	8.27	−76.4	−14.8	−11.5	2.8	−95.6	
	1	4.11	43.4	−2.9	−2.6	0.0	40.1	
	1	7.88	15.2	−2.7	−5.5	0.4	9.1	
	1	8.55	−10.7	−0.6	−0.3	0.0	−11.6	
	1	7.63	−57.3	−6.7	−4.6	0.0	−66.8	
	1	4.30	−57.3	−6.7	−4.6	0.0	−66.8	
	1	3.97	43.4	−2.9	−2.6	0.0	40.1	
			−148	−63.4	−66.5	17.8	−237	
5								
	1	4.81	44.8	−37.4	−40.7	16.9	−1.7	$-x, -y, -z$
	1	7.06	−3.7	−0.6	−1.3	0.0	−5.2	
	1	5.38	10.1	−0.5	−0.7	0.0	9.3	
	1	8.75	0.0	−6.4	0.0	0.0	−4.1	$-x, -y, -z$
	1	5.87	10.7	−1.4	−1.5	0.0	8.6	
	1	6.64	−13.6	−9.5	−10.7	2.6	−27.6	
	1	7.38	−39.5	−4.5	−7.6	0.5	−49.7	$-x, -y, -z$
	1	7.29	44.8	−37.4	−40.7	16.9	−1.7	
	1	4.83	4.5	−0.2	−0.2	0.0	4.3	
	1	6.01	−13.6	−9.5	−10.7	2.6	−27.6	
	1	6.96	10.7	−1.4	−1.5	0.0	8.6	
			55.2	−108.8	−115.6	39.5	−86.8	
6								
	2	7.91	−123.7	−40.9	−8.7	74	−100.5	$-x, y+1/2, -z+1/2$
	1	6.17	−16.6	−2.4	−1.7	0.0	−19.9	
	2	9.34	−16.6	−2.4	−1.7	0.0	−19.9	$x, -y+1/2, z+1/2$
	1	8.06	28.9	−1.4	−0.5	0.0	28.1	
	1	6.45	−123.7	−40.9	−8.7	74	−100.5	
	1	6.94	0.0	−0.1	0.0	0.0	−0.1	
	1	9.53	−16.6	−2.4	−1.7	0.0	−19.9	
	1	9.60	0.0	−0.3	0.0	0.0	−0.2	
	1	9.73	−123.7	−40.9	−8.7	74	−100.5	
			−392	−131.7	−31.7	222	−333.4	
			Energy model		k_ele	k_pol	k_disp	k_rep
			CE-HF···HF/3-21G electron densities		1.019	0.651	0.901	0.811
			CE-B3LYP···B3LYP/6-31G(d,p) electron densities		1.057	0.740	0.871	0.618

k—scale factor. Each form of energy should be multiplied by its relevant factor.

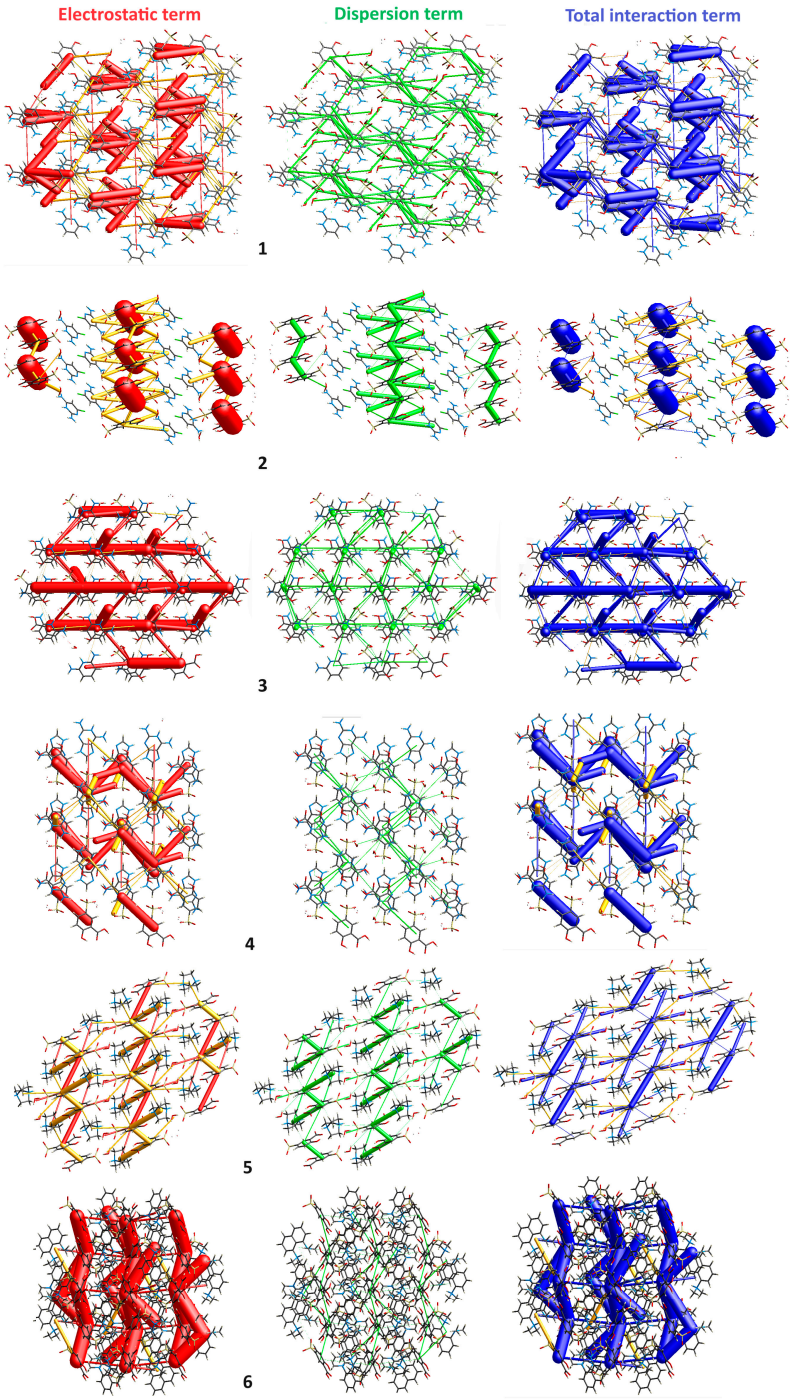

Figure 13. A comparison of energy frameworks in crystals **1**–**6** presented in a cluster (a radius of 3.8 Å) viewed down the a-axis.

4. Conclusions

In summary, a series of novel salts of heterocyclic polyamines with 5-sulfosalicylic acid, namely 2,4-diaminopyrimidin-1-ium 3-carboxy-4-hydroxybenzenesulfonate dihydrate (**1**), 2,4-diamino-6-chloropyrimidin-1-ium 3-carboxy-4-hydroxybenzenesulfonate hydrate (**2**), 2,6-diaminopyridin-1-ium 3-carboxy-4-hydroxybenzenesulfonate monohydrate (**3**), 2,6-diamino-9*H*-purin-1-ium 3-carboxy-4-hydroxybenzenesulfonate monohydrate (**4**), and 8-(dimethylamino)-*N*,*N*-dimethylnaphthalen-1-aminium 3-carboxy-4-hydroxybenzenesulfonate (**6**) have been reported for the first time, to the best of our knowledge. We managed to successfully synthesize and crystallize new salts and determine their crystal structures

by single-crystal X-ray diffraction. The hierarchical supramolecular features were characterized by diverse modern approaches, including mainly extended Hirshfeld surface concepts. In addition, in the analysis, we included 1,4-diazabicyclo[2.2.2]octane-1,4-dium 2-hydroxy-5-sulfonatobenzoate monohydrate (**5**) as a better re-determination of its previously published equivalent (CSD refcode: KAXAE). The new compounds **1**, **2**, **4**, and **5** crystallize in the triclinic $P\bar{1}$ space group, while compounds **3** and **6** crystallize in the monoclinic $P2_1$ and $P2_1/c$ space groups, respectively. Differences in the intermolecular interactions in **1**–**6** were seen on the Hirshfeld surface maps and fingerprint plots, as well as the energy frameworks. More specifically, O···H/H···O interactions are significant contributors (~ 50%). However, C···H/H···C (5–23%) N···H/H···N (below 7%) and C···C (below 10%) inter-contacts also govern the crystal packing of the studied structures. The latter represents π···π contacts with the shortest interplanar distance of 3.4111(12) Å in **4**. The electrostatic interactions in most crystals (in **1**, **3**, **4**, and **6**), while the dispersion forces only in **2** and **5,** were regarded as dominant in stabilizing the crystal packing. Notably, the presence of water molecules has a pivotal role in determining the crystal packing, as either a donor or acceptor, as well as, to some extent, the electrostatic properties. A library of hierarchical supramolecular H-bonding motifs is provided. A specific intramolecular synthon via O-H···O is observed in nearly all crystals. It can be employed in the pseudo-cyclic replacement strategy in the design of new molecules.

Supplementary Materials: The following supporting information can be downloaded at: https://www.mdpi.com/article/10.3390/cryst14060497/s1. Figure S1. Other types of supramolecular H-bonding motifs observed in crystals **1**–**6**. Figure S2. The ATR-FTIR spectrum of **1**. Figure S3. The ATR-FTIR spectrum of **2**. Figure S4. The ATR-FTIR spectrum of **3**. Figure S5. The ATR-FTIR spectrum of **4**. Figure S6. The ATR-FTIR spectrum of **5**. Figure S7. The ATR-FTIR spectrum of **6**. Table S1. Selected bond length and angles of **1**–**6**. Table S2. The π···π interactions (<4.5 Å) in **1**–**6**. Table S3. Other π-based interactions in **1**–**6**. Table S4. Portfolio of selected H-bonding motifs in **1**–**6**. Table S5. Percentage contribution of non-covalent interactions in crystals **1**–**6** based on Hirshfeld surface analysis. Table S6. Enrichment ratios in crystals **1**–**6** based on Hirshfeld surface analysis.

Author Contributions: Conceptualization, A.M. and J.B.; methodology A.M., K.Ł. and J.B.; validation, K.Ł. and J.B.; formal analysis, K.Ł. and J.B.; investigation, K.Ł., J.B. and A.M.; data curation, K.Ł. and J.B.; writing—original draft preparation, K.Ł., J.B. and A.M. All authors have read and agreed to the published version of the manuscript.

Funding: This research received no external funding.

Data Availability Statement: The CIF files have been deposited at the Cambridge Crystallographic Data Centre (CCDC) with the following numbers: 2348280–2348285, accessed on 15 May 2024. These data can be obtained free of charge via https://www.ccdc.cam.ac.uk/structures.

Conflicts of Interest: The authors declare no conflicts of interest.

References

1. Ganie, A.A.; Vishnoi, P.; Dar, A.A. Utility of Bis-4-pyridines as Supramolecular Linkers for 5-Sulfosalicylic Acid Centers: Structural and Optical Investigations. *Cryst. Growth Des.* **2019**, *19*, 2289–2297. [CrossRef]
2. Wu, Y.; Hao, X.; Li, J.; Guan, A.; Zhou, Z.; Guo, F. New insight into improving the solubility of poorly soluble drugs by preventing the formation of their hydrogen-bonds: A case of dapsone salts with camphorsulfonic and 5-sulfosalicylic acid. *CrystEngComm* **2021**, *23*, 6191–6198. [CrossRef]
3. Du, H.; Xu, L.; Yue, M.; Xu, F.; Wang, Y. Studies on crystal structures, optical, solubility and dyeing properties of two new crystalline dye salts based on berberine with aromatic carboxylic acid. *J. Mol. Struct.* **2022**, *1260*, 132856. [CrossRef]
4. Zhang, Y.-N.; Duan, Y.; Liu, L.-X.; Chang, L.; Feng, Y.-R.; Wu, L.-L.; Zhang, L.; Zhang, Y.-J.; Zou, D.-Y.; Liu, Y.-L.; et al. On improving the hygroscopic stability of palmatine chloride with crystalline palmatine sulfosalicylate pharmaceutical salt. *J. Struct. Chem.* **2022**, *63*, 52–61. [CrossRef]
5. Hua, X.-N.; Pan, X.; Zhu, Y.; Cai, Z.; Song, Q.; Li, Y.; Feng, W.; Chen, X.; Zhang, H.; Sun, B. Novel pharmaceutical salts of cephalexin with organic counterions: Structural analysis and properties. *RSC Adv.* **2022**, *12*, 34843–34850. [CrossRef] [PubMed]
6. Dar, A.A.; Lone, S.H.; Ahmad, I.; Ahangar, A.A.; Ganie, A.A.; Femina, C. Engineering the solid-state luminescence of organic crystals and cocrystals. *Mater. Adv.* **2024**, *5*, 1056–1064. [CrossRef]

7. Duan, W.; Liu, B.; Gong, N.; Famulari, A.; Guo, F. Polymorphs and Transformations of the Solid Forms of Organic Salts of 5-Sulfosalicylic Acid and Isonicotinamide. *Cryst. Growth Des.* **2020**, *20*, 7606–7614. [CrossRef]
8. Ganie, A.A.; Ismail, T.M.; Sajith, P.K.; Dar, A.A. Validation of the supramolecular synthon preference through DFT and physico-chemical property investigations of pyridyl salts of organo-sulfonates. *New J. Chem.* **2021**, *45*, 4780–4790. [CrossRef]
9. Ganie, A.A.; Marimuthu, R.; Islam, S.T.; Narang, S.; Dar, A.A. Molecular salts of the isoniazid derivatives. Expanding the scope of sulfonate-pyridinium synthon to design materials. *J. Solid State Chem.* **2022**, *307*, 122762. [CrossRef]
10. Ramesh, K.S.; Saravanabhavan, M.; Muhammad, S.; Edison, D.; Ho, M.-S.; Sekar, M.; Al-Sehemi, A.G. Synthesis, physico-chemical characterization and quantum chemical studies of 2, 3-dimethyl quinoxalinium-5-sulphosalicylate crystal. *J. Mol. Struct.* **2023**, *1285*, 135425. [CrossRef]
11. Smith, G.; Wermuth, U.D. Hydrogen bonding in two ammonium salts of 5-sulfosalicylic acid: Ammonium 3-carboxy-4-hydroxybenzenesulfonate monohydrate and triammonium 3-carboxy-4-hydroxybenzenesulfonate 3-carboxylato-4-hydroxybenzenesulfonate. *Acta Crystallogr. Sect. C Cryst. Struct. Commun.* **2013**, *69*, 534–537. [CrossRef]
12. Selvaraju, D.; Venkatesh, R.; Sundararajan, V. Hydrazine-1,2-diium bis(3-carboxy-4-hydroxybenzenesulfonate) tetrahydrate. *Acta Crystallogr. Sect. E Struct. Rep. Online* **2011**, *67*, o1236–o1237. [CrossRef]
13. Smith, G.; Wermuth, U.D.; Healy, P.C. Hydrogen bonding in proton-transfer compounds of 5-sulfosalicylic acid with *ortho*-substituted monocyclic heteroaromatic Lewis bases. *J. Chem. Crystallogr.* **2006**, *36*, 841–849. [CrossRef]
14. Raj, S.B.; Sethuraman, V.; Francis, S.; Hemamalini, M.; Muthiah, P.T.; Bocelli, G.; Cantoni, A.; Rychlewska, U.; Warzajtis, B. Supramolecular organization via hydrogen bonding in trimethoprim sulfonate salts. *CrystEngComm* **2003**, *5*, 70–76. [CrossRef]
15. Hemamalini, M.; Muthiah, P.T.; Sridhar, B.; Rajaram, R.K. Pyrimethaminium sulfosalicylate monohydrate. *Acta Crystallogr. Sect. E Struct. Rep. Online* **2005**, *61*, o1480–o1482. [CrossRef]
16. Matulkova, I.; Mathauserova, J.; Cisarova, I.; Nemec, I.; Fabry, J. The study of crystal structures and vibrational spectra of inorganic salts of 2,4-diaminopyrimidine. *J. Mol. Struct.* **2016**, *1103*, 82–93. [CrossRef]
17. Bertolasi, V.; Pretto, L.; Gilli, P.; Ferretti, V.; Gilli, G. Hydrogen-bonded supramolecular structures in co-crystals of β- or ζ-diketone enols with 2,6-diaminopyridine or 2,4-diaminopyrimidine. *New J. Chem.* **2002**, *26*, 1559–1566. [CrossRef]
18. Draguta, S.; Fonari, M.S.; Masunov, A.E.; Zazueta, J.; Sullivan, S.; Antipin, M.Y.; Timofeeva, T.V. New acentric materials constructed from aminopyridines and 4-nitrophenol. *CrystEngComm* **2013**, *15*, 4700–4710. [CrossRef]
19. Hutzler, W.M.; Egert, E.; Bolte, M. 6-Propyl-2-thiouracil versus 6-methoxymethyl-2-thiouracil: Enhancing the hydrogen-bonded synthon motif by replacement of a methylene group with an O atom. *Acta Crystallogr. Sect. C Cryst. Struct. Commun.* **2016**, *72*, 634–646. [CrossRef]
20. Hutzler, W.M.; Egert, E.; Bolte, M. One barbiturate and two solvated thiobarbiturates containing the triply hydrogen-bonded ADA/DAD synthon, plus one ansolvate and three solvates of their coformer 2,4-diaminopyrimidine. *Acta Cryst. C* **2016**, *72*, 705–715. [CrossRef]
21. Hall, V.M.; Thornton, A.; Miehls, E.K.; Bertke, J.A.; Swift, J.A. Uric Acid Crystallization Interrupted with Competing Binding Agents. *Cryst. Growth Des.* **2019**, *19*, 7363–7371. [CrossRef]
22. Bojarska, J.; Łyczko, K.; Mieczkowski, A. Synthesis, Crystal Structure and Supramolecular Features of Novel 2,4-Diaminopyrimidine Salts. *Crystals* **2024**, *14*, 133. [CrossRef]
23. Smith, G.; Wermuth, U.D.; Healy, P.C. Layered structures in proton-transfer compounds of 5-sulfosalicylic acid with the aromatic polyamines 2,6-diaminopyridine and 1,4-phenylenediamine. *Acta Crystallogr. Sect. C Cryst. Struct. Commun.* **2005**, *61*, o555–o558. [CrossRef] [PubMed]
24. Hemamalini, M.; Goh, J.H.; Fun, H.-K. 2,3-Diaminopyridinium 3-carboxy-4-hydroxybenzenesulfonate monohydrate. *Acta Crystallogr. Sect. E Struct. Rep. Online* **2011**, *67*, o3122. [CrossRef] [PubMed]
25. Hemamalini, M.; Fun, H.-K. 2-Amino-5-chloropyridinium 3-carboxy-4-hydroxybenzenesulfonate. *Acta Crystallogr. Sect. E Struct. Rep. Online* **2010**, *66*, o2323–o2324. [CrossRef] [PubMed]
26. Manickam, R.; Rajakannan, V.; Prabhaharan, M.; Srinivasan, G. 2-Amino-6-chloropyridinium 3-carboxy-4-hydroxybenzenesulfonate. *IUCrData* **2019**, *4*, x190566. [CrossRef]
27. Hemamalini, M.; Fun, H.-K. 2-Amino-5-bromopyridinium 3-carboxy-4-hydroxybenzenesulfonate. *Acta Crystallogr. Sect. E Struct. Rep. Online* **2010**, *66*, o2408–o2409. [CrossRef] [PubMed]
28. Hemamalini, M.; Fun, H.-K. 2-Amino-5-methylpyridinium 3-carboxy-4-hydroxybenzenesulfonate. *Acta Crystallogr. Sect. E Struct. Rep. Online* **2010**, *66*, o2153–o2154. [CrossRef]
29. Atria, A.M.; Garland, M.T.; Baggio, R. 2,6-Diamino-9*H*-purine monohydrate and bis(2,6-diamino-9*H*-purin-1-ium) 2-(2-carboxylatophenyl)acetate heptahydrate: Two simple structures with very complex hydrogen-bonding schemes. *Acta Crystallogr. Sect. C Cryst. Struct. Commun.* **2010**, *66*, o547–o552. [CrossRef]
30. Belletire, J.L.; Schneider, S.; Shackelford, S.A.; Peryshkov, D.V.; Strauss, S.H. Pairing heterocyclic cations with *closo*-dodecafluorododecaborate (2−): Synthesis of binary heterocyclium(1+) salts and a $Ag_4(heterocycle)_8^{4+}$ salt of $B_{12}F_{12}^{2-}$. *J. Fluor. Chem.* **2011**, *132*, 925–936. [CrossRef]
31. de Vries, E.J.C.; Kantengwa, S.; Ayamine, A.; Báthori, N.B. Testing the limits of synthon engineering: Salts of salicylic and sulfosalicylic acid with nucleobases and derivatives. *CrystEngComm* **2016**, *18*, 7573–7579. [CrossRef]
32. Xia, M.; Ma, K.-R.; Zhu, Y. Synthesis and Crystal Structure of Hydrate Adduct of 6-Benzylaminopurine and 5-Sulfosalicylic Acid $[(C_{12}H_{12}N_5)(C_7H_5O_6S)\cdot H_2O]$. *J. Chem. Crystallogr.* **2010**, *40*, 634–638. [CrossRef]

33. Jones, A.O.F.; Kallay, A.A.; Lloyd, H.; McIntyre, G.J.; Wilson, C.C.; Thomas, L.H. The Effect of Local Crystalline Environment on Hydrogen Atom Behavior in Molecular Complexes of a Proton Sponge. *Cryst. Growth Des.* **2016**, *16*, 2123–2129. [CrossRef]
34. Sigala, P.A.; Ruben, E.A.; Liu, C.W.; Piccoli, P.M.B.; Hohenstein, E.G.; Martinez, T.J.; Schultz, A.J.; Herschlag, D. Determination of Hydrogen Bond Structure in Water versus Aprotic Environments To Test the Relationship Between Length and Stability. *J. Am. Chem. Soc.* **2015**, *137*, 5730–5740. [CrossRef] [PubMed]
35. Ye, H.-Y.; Tang, Y.-Y.; Li, P.-F.; Liao, W.-Q.; Gao, J.-X.; Hua, X.-N.; Cai, H.; Shi, P.-P.; You, Y.-M.; Xiong, R.-G. Metal-free three-dimensional perovskite ferroelectrics. *Science* **2018**, *361*, 151–155. [CrossRef] [PubMed]
36. Jiang, X.; Duan, H.-B.; Jellen, M.J.; Chen, Y.; Chung, T.S.; Liang, Y.; Garcia-Garibay, M.A. Thermally Activated Transient Dipoles and Rotational Dynamics of Hydrogen-Bonded and Charge-Transferred Diazabicyclo [2.2.2]Octane Molecular Rotors. *J. Am. Chem. Soc.* **2019**, *141*, 16802–16809. [CrossRef]
37. Song, X.; Cui, Q.; Liu, Y.; Xu, Z.; Cohen, H.; Ma, C.; Fan, Y.; Zhang, Y.; Ye, H.; Peng, Z.; et al. Metal-Free Halide Perovskite Single Crystals with Very Long Charge Lifetimes for Efficient X-ray Imaging. *Adv. Mater.* **2020**, *32*, 2003353. [CrossRef] [PubMed]
38. Chu, L.-L.; Zhang, T.; Zhang, W.-Y.; Shi, P.-P.; Gao, J.-X.; Ye, Q.; Fu, D.-W. Three-Dimensional Metal-Free Molecular Perovskite with a Thermally Induced Switchable Dielectric Response. *J. Phys. Chem. Lett.* **2020**, *11*, 1668–1674. [CrossRef]
39. Budzianowski, A.; Petříček, V.; Katrusiak, A. Metal-free enantiomorphic perovskite $[dabcoH_2]_2^+[H_3O]^+Br_3^-$ and its one-dimensional polar polymorph. *IUCrJ* **2022**, *9*, 544–550. [CrossRef]
40. Song, X.; Cohen, H.; Yin, J.; Li, H.; Wang, J.; Yuan, Y.; Huang, R.; Cui, Q.; Ma, C.; Liu (Frank), S.; et al. Low Dimensional, Metal-Free, Hydrazinium Halide Perovskite-Related Single Crystals and Their Use as X-Ray Detectors. *Small* **2023**, *19*, 2300892. [CrossRef]
41. Jin, S.; Guo, J.; Liu, L.; Wang, D. Five organic salts assembled from carboxylic acids and bis-imidazole derivatives through collective noncovalent interactions. *J. Mol. Struct.* **2011**, *1004*, 227–236. [CrossRef]
42. Guo, F.; Zhang, M.-Q.; Famulari, A.; Marti-Rujas, J. Solid state transformations in stoichiometric hydrogen bonded molecular salts: Ionic interconversion and dehydration processes. *CrystEngComm* **2013**, *15*, 6237–6243. [CrossRef]
43. Liu, H.-l.; Xie, Y.-F.; Pan, Z.-G.; Famulari, A.; Guo, F.; Zhou, Z.; Martí-Rujas, J. Cyclic Interconversion among Molecular Salts via Neat Grinding and Related Photoluminescence Properties. *Cryst. Growth Des.* **2014**, *14*, 6528–6536. [CrossRef]
44. Fu, Q.; Xu, X.-K.; Liu, B.-K.; Guo, F. Solid state transformations of different stoichiometric forms of an organic salt formed from 5-sulfosalicylic acid and hexamethylenetetramine upon dehydration and rehydration. *CrystEngComm* **2018**, *20*, 1844–1852. [CrossRef]
45. Yang, D.-J.; Qu, S.-H. Bis(2-aminopyridinium) 5-sulfonatosalicylate. *Acta Crystallogr. Sect. E Struct. Rep. Online* **2006**, *62*, o5127–o5129. [CrossRef]
46. Jin, S.; Zhao, Y.; Liu, B.; Jin, X.; Zhang, H.; Wen, X.; Liu, H.; Jin, L.; Wang, D. Hydrogen bonded supramolecular structures of eight organic salts based on 2,6-diaminopyridine, and organic acids. *J. Mol. Struct.* **2015**, *1099*, 601–615. [CrossRef]
47. Balasubramani, K.; Muthiah, P.T.; Lynch, D.E. $R_2^2(8)$ motifs in aminopyrimidine sulfonate/carboxylate interactions: Crystal structures of pyrimethaminium benzenesulfonate monohydrate (2:2:1) and 2-amino-4,6-dimethylpyrimidinium sulfosalicylate dihydrate (4:2:2). *Chem. Cent. J.* **2007**, *1*, 28. [CrossRef] [PubMed]
48. Jin, S.; Jin, L.; Ye, X.; Li, J.; Jin, B.; Zheng, L.; Wang, D. Crystal and Molecular Structure of Three Organic Salts from N^6-Benzyladenine, 5-Sulfosalicylic Acid, Naphthalene-1,5-Disulfonic Acid, and α-Ketoglutaric Acid. *J. Chem. Crystallogr.* **2015**, *45*, 9–19. [CrossRef]
49. Krishnamohan, S.C.V. Crystal engineering—-Where do we go from here? *Cryst. Growth Des.* **2002**, *2*, 465–474. [CrossRef]
50. Braga, D.; Brammer, L.; Champness, N.R. New trends in crystal engineering. *CrystEngComm* **2005**, *7*, 1–19. [CrossRef]
51. Bond, A.D.; Jones, W. *Supramolecular Organization And Materials Design*; Cambridge University Press: Cambridge, UK, 2002.
52. Desiraju, G.R. Supramolecular Synthons in Crystal Engineering—A New Organic Synthesis. *Angew. Chem. Int. Ed. Engl.* **1995**, *34*, 2311–2327. [CrossRef]
53. Walsh, R.D.B.; Bradner, M.W.; Fleischman, S.; Morales, L.A.; Moulton, B.; Rodríguez-Hornedo, N.; Zaworotko, M.J. Crystal Engineering of the Composition of Pharmaceutical Phases. *Chem. Commun.* **2003**, *2*, 186–187. [CrossRef]
54. Bojarska, J.; Breza, M.; Remko, M.; Yuan, Y.; Ziora, Z.; Chai, T.-T.; Madura, I.D.; Kaczmarek, K.; Blaskovich, M.A.T.; Wolf, M.W. A supramolecular self-assembly of peptide-derived compounds via 1,5-disubstituted tetrazole-based supramolecular synthons: An experimental and computational study. *J. Mol. Struct.* **2023**, *1288*, 135732. [CrossRef]
55. Bojarska, J.; Breza, M.; Remko, M.; Borowiecki, P.; Fruziński, A.; Madura, I.D.; Kaczmarek, K.; Leśnikowski, Z.; Kraj, A.; Zielenkiewicz, P.; et al. Supramolecular synthon hierarchy in cyclopropyl containing peptide-derived compounds. *CrystEngComm* **2022**, *24*, 8372–8389. [CrossRef]
56. Bojarska, J.; Breza, M.; Remko, M.; Czyz, M.; Gajos-Michniewicz, A.; Zimecki, M.; Kaczmarek, K.; Madura, I.D.; Wojciechowski, J.M.; Wolf, W.M. Structural and Biofunctional Insights into the Cyclo(Pro-Pro-Phe-Phe-)Scaffold from Experimental and In Silico Studies: Melanoma and Beyond. *Int. J. Mol. Sci.* **2022**, *23*, 7173. [CrossRef]
57. Bojarska, J.; Remko, M.; Madura, I.D.; Kaczmarek, K.; Zabrocki, J.; Wolf, W.M. Synthesis, experimental and in silico studies of *N*-fluorenylmethoxycarbonyl-*O*-*tert*-butyl-*N*-methyltyrosine, coupled with CSD data: A survey of interactions in the crystal structures of Fmoc-amino acids. *Acta Crystallogr. C* **2020**, *76*, 328–345. [CrossRef]
58. Sheldrick, G.M. Crystal Structure Refinement with SHELXL. *Acta Cryst. C Struc. Chem.* **2015**, *71*, 3–8. [CrossRef] [PubMed]

59. Dolomanov, O.V.; Bourhis, L.J.; Gildea, R.J.; Howard, J.A.K.; Puschmann, H. OLEX2: A complete structure solution, refinement and analysis program. *J. Appl. Crystallogr.* **2009**, *42*, 339–341. [CrossRef]
60. Macrae, C.F.; Sovago, I.; Cottrell, S.J.; Galek, P.T.A.; McCabe, P.; Pidcock, E.; Platings, M.; Shields, G.P.; Stevens, J.S.; Towler, M.; et al. Mercury 4.0: From visualization to analysis, design and prediction. *J. Appl. Cryst.* **2020**, *53*, 226–235. [CrossRef]
61. Spek, A.L. Structure Validation in chemical crystallography. *Acta Cryst. D Biol. Crystallogr.* **2009**, *65*, 148–155. [CrossRef]
62. Wood, P.A.; Olsson, T.S.G.; Cole, J.C.; Cottrell, S.J.; Feeder, N.; Galek, P.T.A.; Groom, C.R.; Pidcock, E. Evaluation of Molecular Crystal Structures Using Full Interaction Maps. *CrystEngComm* **2013**, *15*, 65–72. [CrossRef]
63. Turner, M.J.; McKinnon, J.J.; Wol, S.K.; Grimwood, D.J.; Spackman, P.R.; Jayatilaka, D.; Spackman, M.A. *CrystalExplorer, Version 3.1*; The University of Western Australia: Perth, Australia, 2017.
64. Spackman, M.A.; Jayatilaka, D. Hirshfeld surface analysis. *CrystEngComm* **2009**, *11*, 19–32. [CrossRef]
65. Jayatilaka, D.; Grimwood, D.J. Tonto: A Fortran Based Object-Oriented System for Quantum Chemistry and Crystallography. In *Computational Science—ICCS 2003*; Sloot, P.M.A., Abramson, D., Bogdanov, A.V., Gorbachev, Y.E., Dongarra, J.J., Zomaya, A.Y., Eds.; Lecture Notes in Computer Science; Springer: Berlin/Heidelberg, Germany, 2003; Volume 2660, pp. 142–151. [CrossRef]
66. Spackman, P.R.; Turner, M.J.; McKinnon, J.J.; Wolff, S.K.; Grimwood, D.J.; Jayatilaka, D.; Spackman, M.A. CrystalExplorer: A program for Hirshfeld surface analysis, visualization and quantitative analysis of molecular crystals. *J. Appl. Crystallogr.* **2021**, *54*, 1006. [CrossRef] [PubMed]
67. Jelsch, C.; Ejsmont, K.; Huder, L. The enrichment ratio of atomic contacts in crystals, an indicator derived from the Hirshfeld surface analysis. *IUCrJ* **2014**, *1*, 119–128. [CrossRef] [PubMed]
68. Spackman, M.A.; McKinnon, J.J. Fingerprinting intermolecular interactions in molecular crystals. *CrystEngComm* **2002**, *4*, 378. [CrossRef]
69. McKinnon, J.J.; Mitchell, A.S.; Spackman, M.A. Hirshfeld Surfaces: A New Tool for Visualizing and Exploring Molecular Crystals. *Chem. Eur. J.* **1998**, *4*, 2136. [CrossRef]
70. Mackenzie, C.F.; Spackman, P.R.; Jayatilaka, D.; Spackman, M.A. CrystalExplorer model energies and energy frameworks: Extension to metal coordination compounds, organic salts, solvates and open-shell systems. *IUCrJ* **2017**, *4*, 575. [CrossRef]
71. Tan, S.L.; Jotani, M.M.; Tiekink, E.R.T. Utilizing Hirshfeld surface calculations, non-covalent interaction (NCI) plots and the calculation of interaction energies in the analysis of molecular packing. *Acta Crystallogr. E Crystallogr. Commun.* **2019**, *75*, 308. [CrossRef]
72. Kitaigorodskii, A.I. *Organic Chemical Crystallography*; Consultants Bureau: New York, NY, USA, 1961; pp. 1–30, 65–112.
73. Kitaigorodskii, A.I. *Molecular Crystals and Molecules*; Academic Press: London, UK, 1973; pp. 1–133.